

# Depósitos eólicos

# Onde desenvolvem-se depósitos eólicos?

- Disponibilidade de areia e silte ==>
- Cobertura vegetal mínima ==>
- Praias, desertos, planícies periglaciais, lagos secos.

# Campos de dunas interiores



Arquitetura

Pré-Vegetação

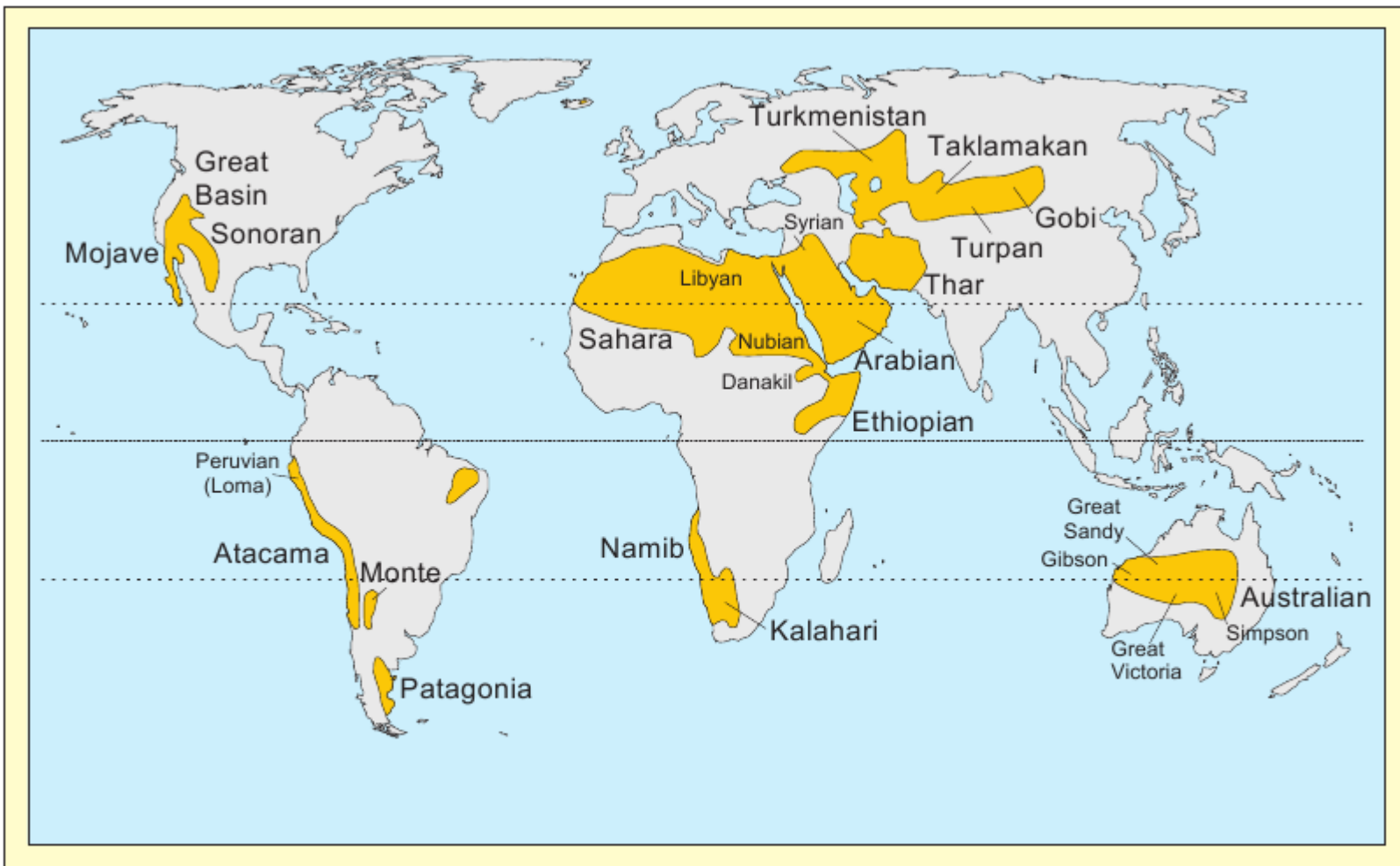


FIG. 1.—Distribution of the world's major climatic deserts.

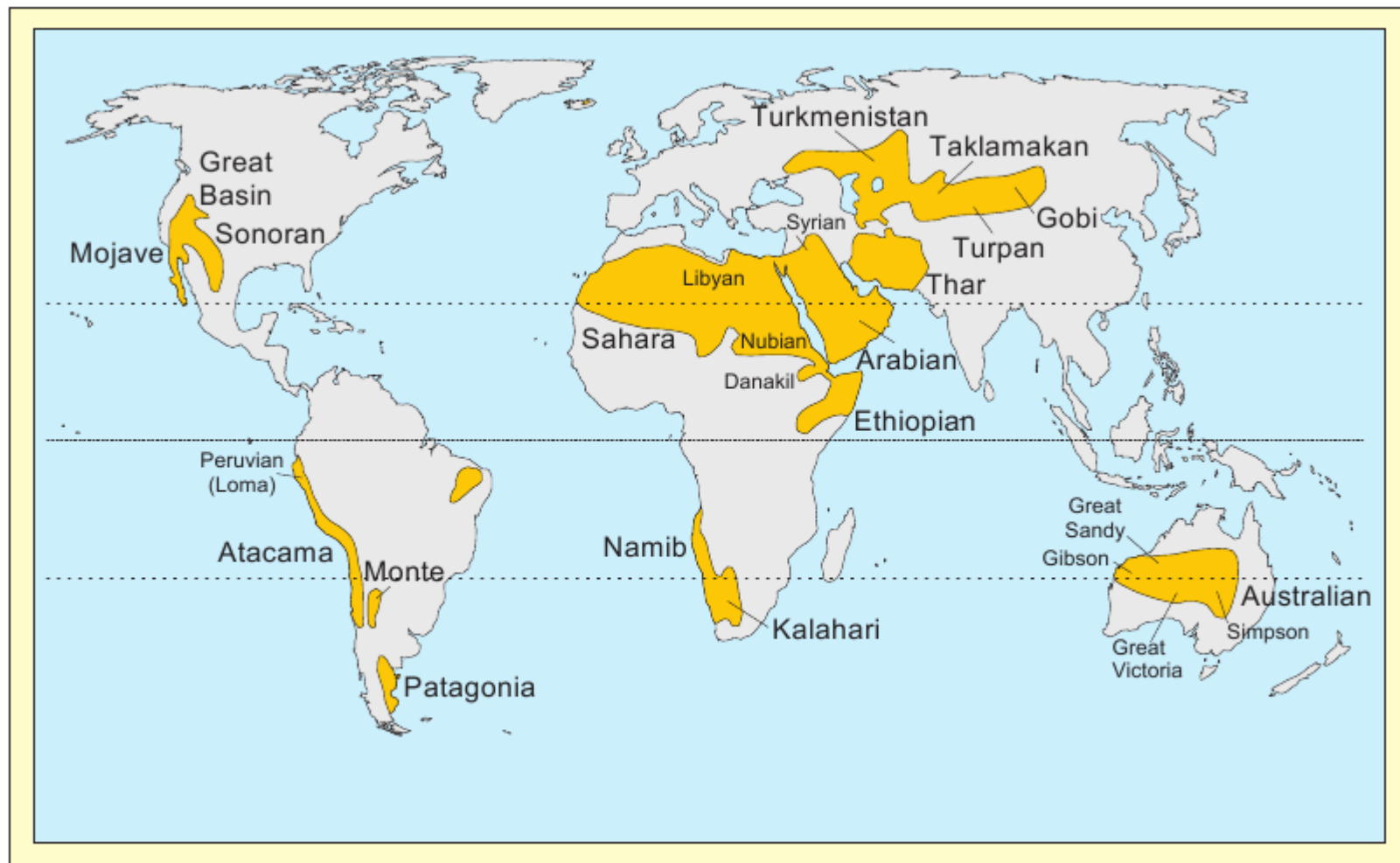
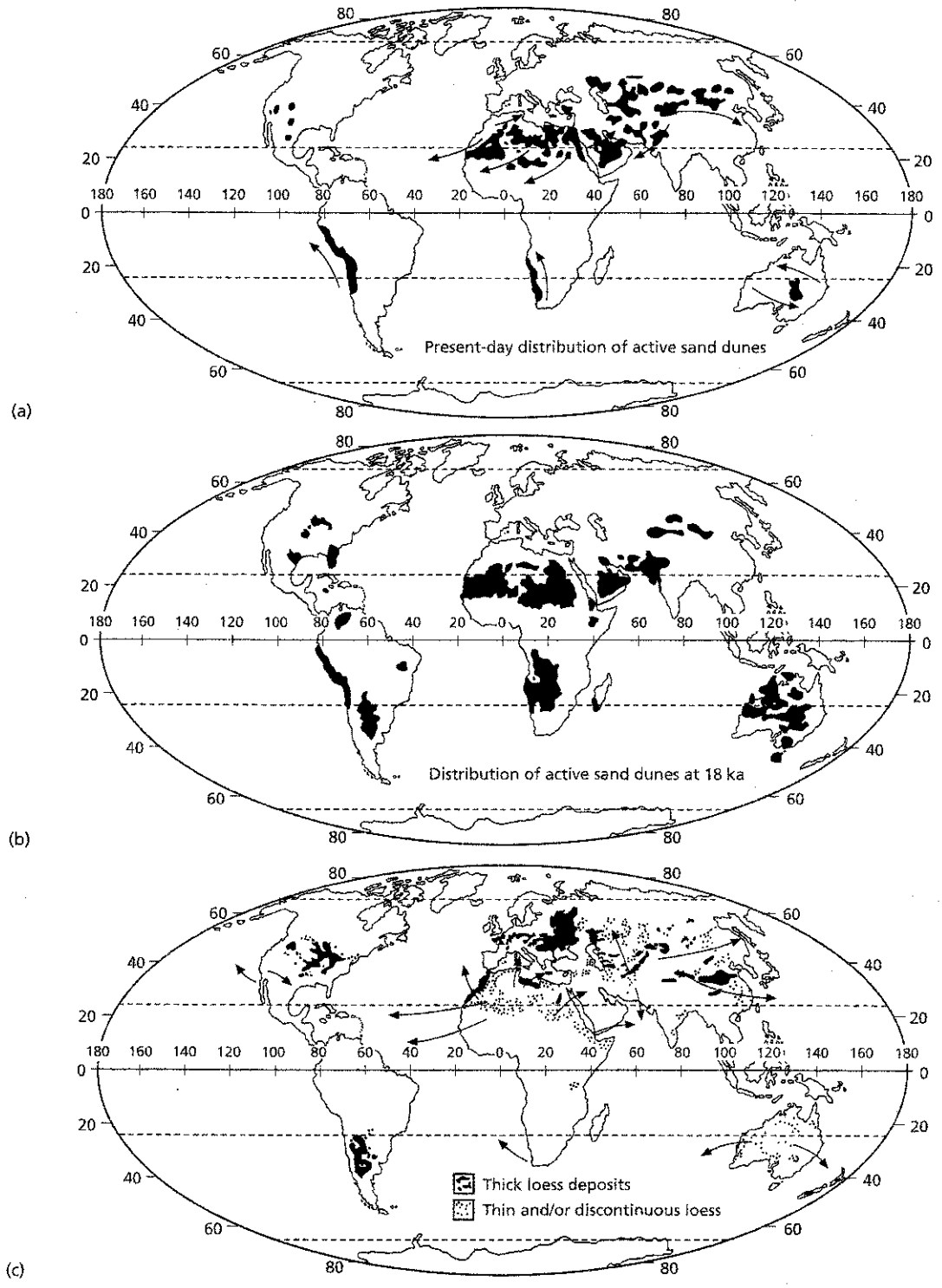


FIG. 1.—Distribution of the world's major climatic deserts.

Planaltos de baixa latitude, áres próximas a correntes oceânicas frias, sobras de chuva.



**Fig. 16.2** Distribution of: (a) present-day active sand dunes and mean dune-forming wind regimes; (b) glacial-maximum active sand dunes; and (c) present-day

distribution of mostly glacial-maximum loess and the mean trajectories of modern aerosol dust tracks. (Mostly after Williams et al., 1993, and sources cited therein.)

## Mudanças climáticas

### Campos de dunas de desertos atuais

### Máximo glacial (18ka)

### Trilhas de loess and poeira de aerosol no máximo glacial

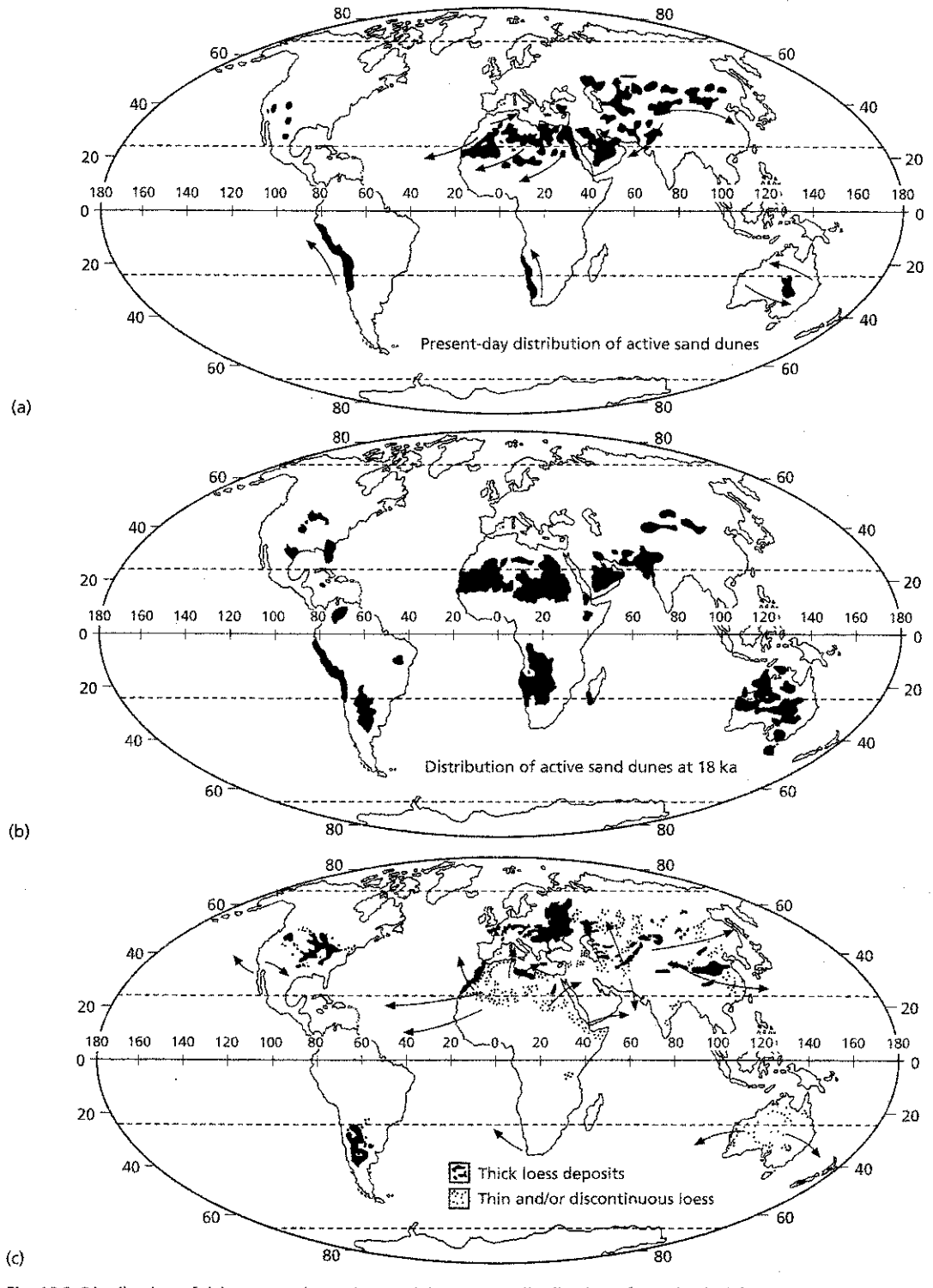
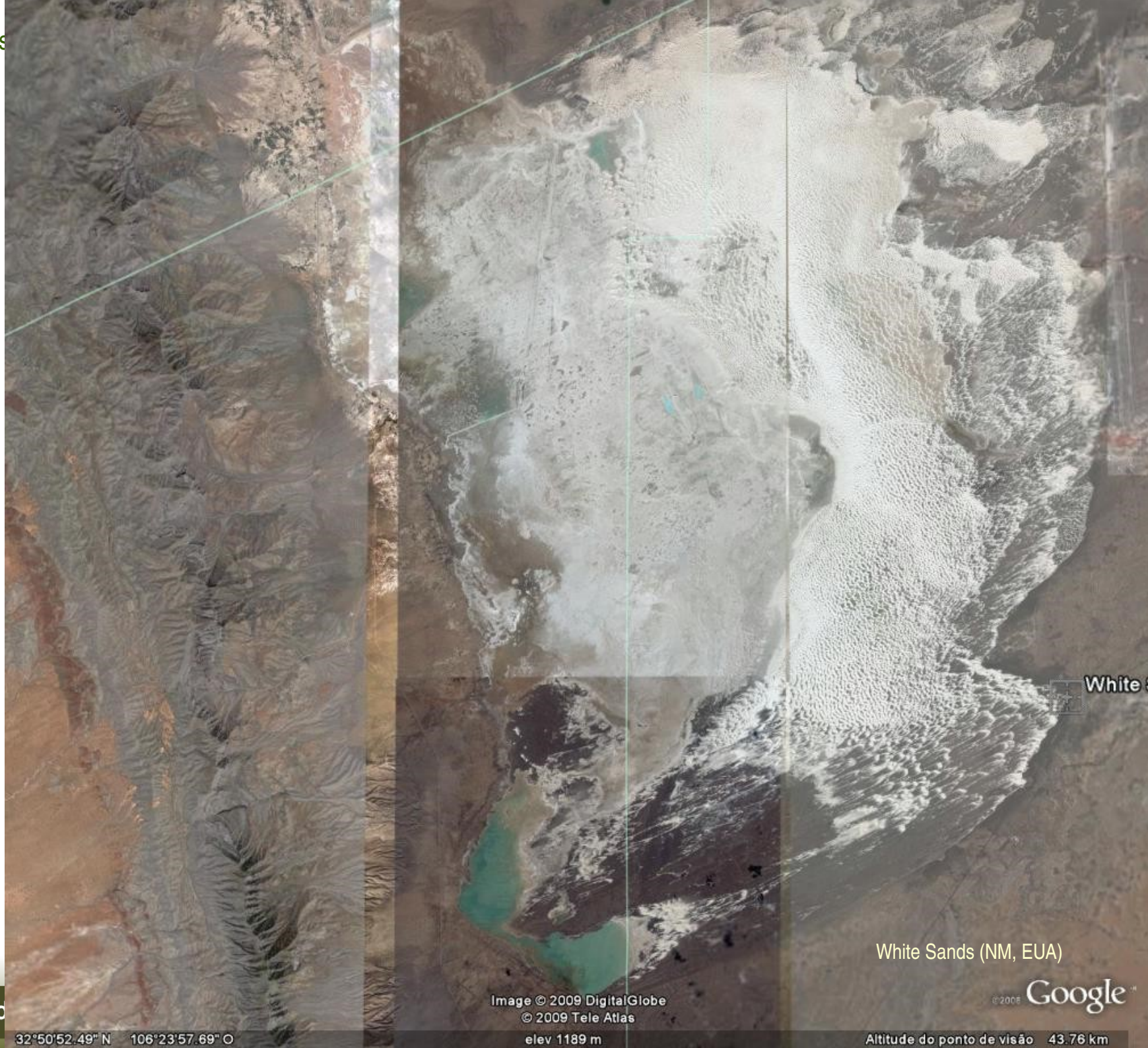


**Fig. 16.2** Distribution of: (a) present-day active sand dunes and mean dune-forming wind regimes; (b) glacial-maximum active sand dunes; and (c) present-day

distribution of mostly glacial-maximum loess and the mean trajectories of modern aerosol dust tracks. (Mostly after Williams et al., 1993, and sources cited therein.)

**Máximo glacial =  
maiores campos de  
dunas!**

**Aridez e energia dos  
ventos aumentadas.**

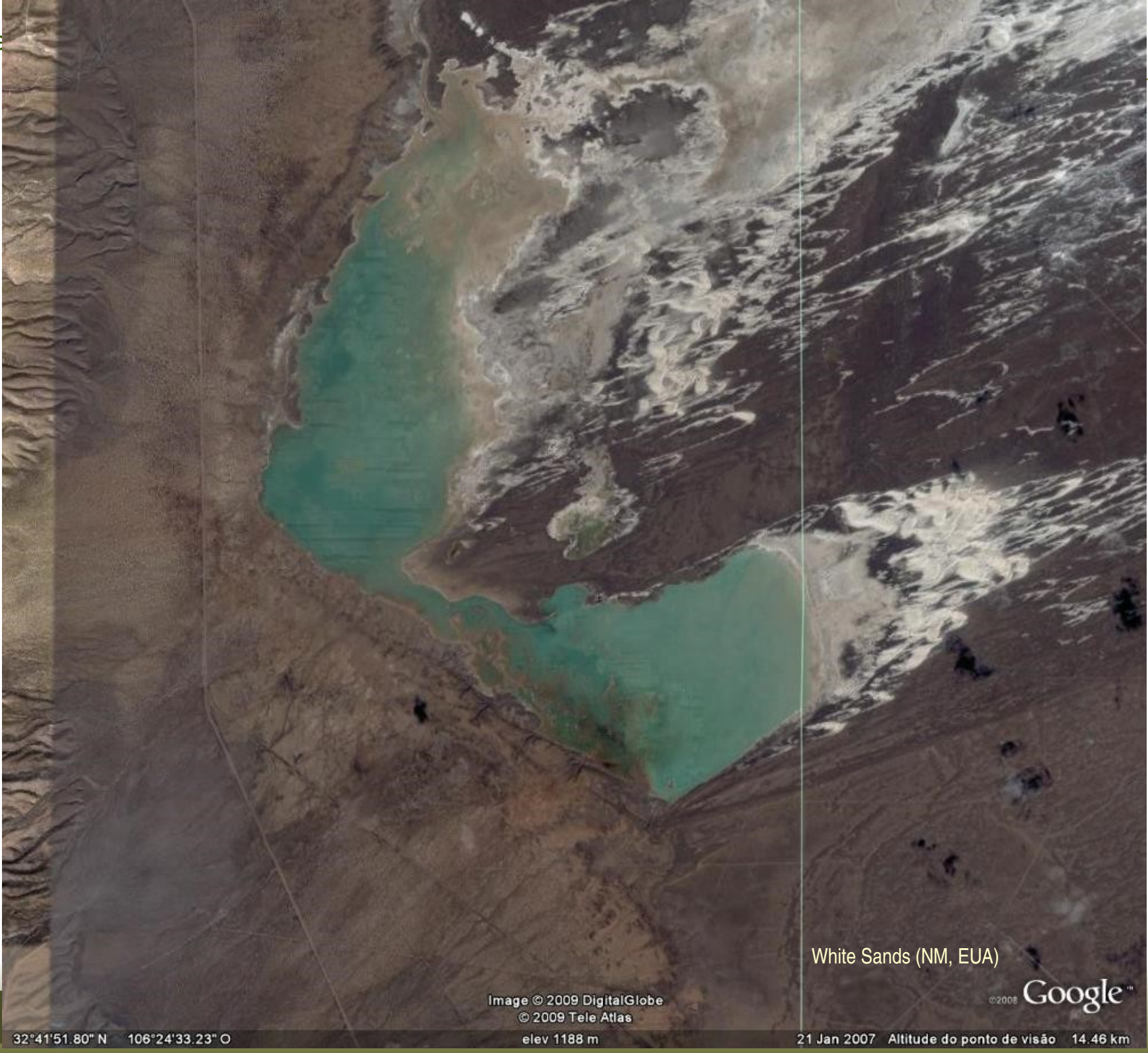


White Sands (NM, EUA)

Image © 2009 DigitalGlobe

© 2009 Tele Atlas

elev 1189 m



White Sands (NM, EUA)

Image © 2009 DigitalGlobe

© 2009 Tele Atlas

elev 1188 m

Google™



White Sands (NM, EUA)

Google

Image © 2009 DigitalGlobe

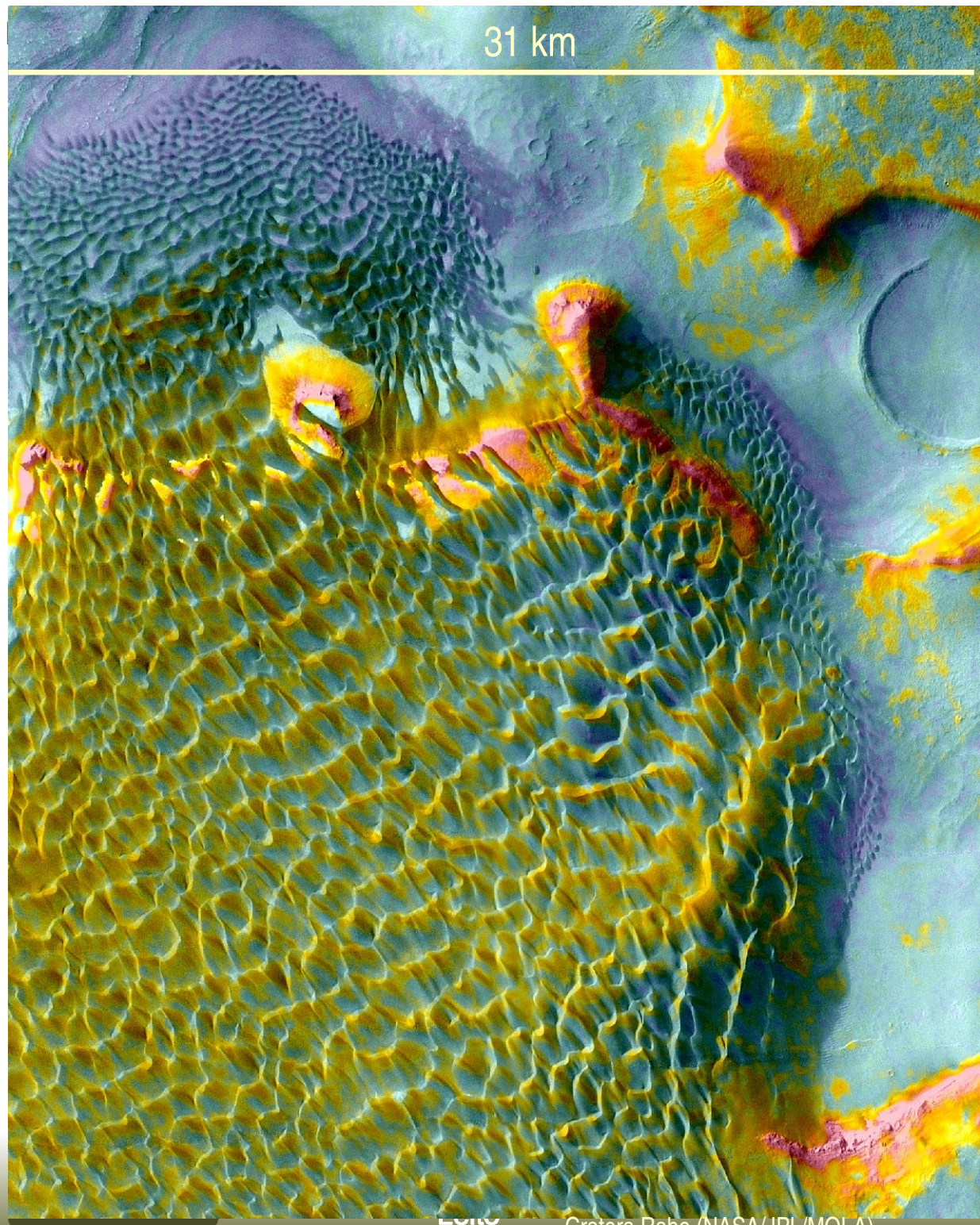
© 2009 Tele Atlas

elev 1219 m

© 2008



31 km



17 km

Arquitetura  
Cratera Proctor (NASA/JPL/MOLA)

Vegetação

# Campos de dunas costeiras



Arquitetura

Pré-Vegetação





Image © 2009 DigitalGlobe

Introd

24°01'45"S 42°36'02.96"E

© 2009 MapLink/Tele Atlas

elev 3 m

15 Out 2005 Altitude do ponto de visão 3.62 km

Google

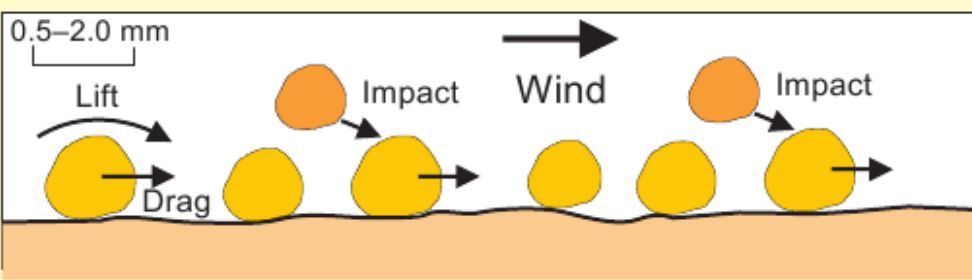
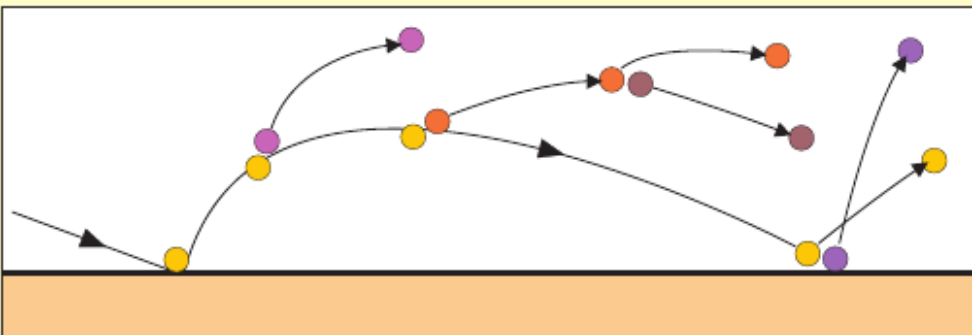
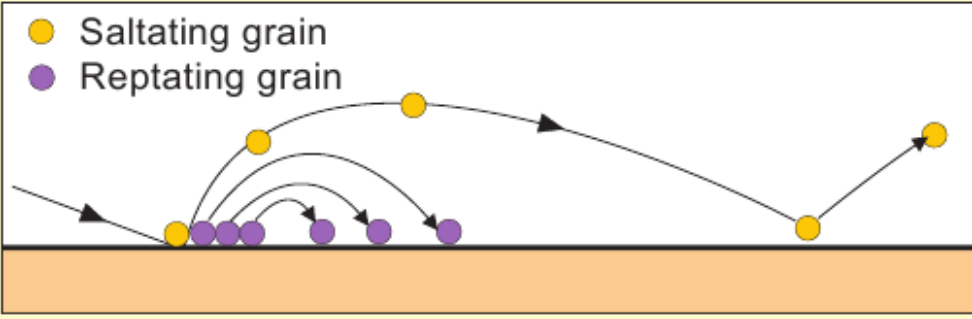
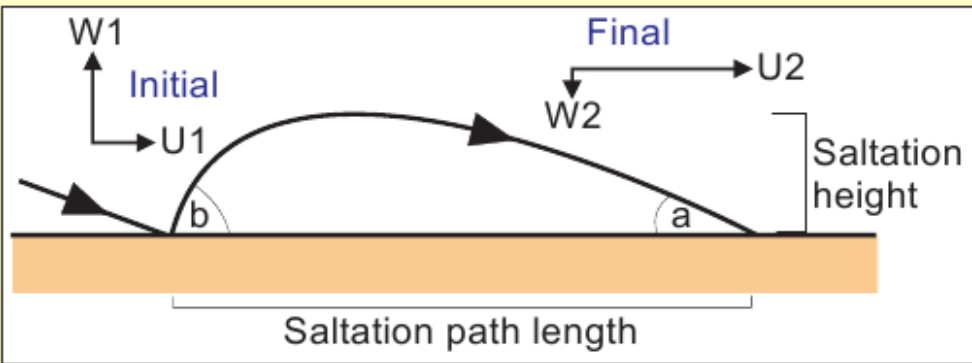
é-  
ação



Image © 2009 DigitalGlobe

# Elementos morfológicos

- Campo de dunas (*erg – sand seas*)
  - Marcas onduladas eólicas ( $H \leq 0.1$  m;  $\lambda = 0.02$  a  $2.0$  m)  $\lambda/H = 25$  a  $40+$
  - Dunas
  - Draas
  - Interdunas
- Lançóis de areia
- Pavimentos de deflação

**A****B****C****D**

Methods of eolian grain transport. A) Surface creep. B) In-air collisions of saltating grains maintains momentum, keeping grains aloft. Ground impacts induce new grains to saltate. C) Impact of saltating grains with grains on bed drives reptation. D)

The ballistic trajectory of a saltating sand grain.  $W$  and  $U$  represent vertical and horizontal velocities, respectively.  $a$  is the approach angle,  $b$  is the take-off angle.

Moutney (2006)

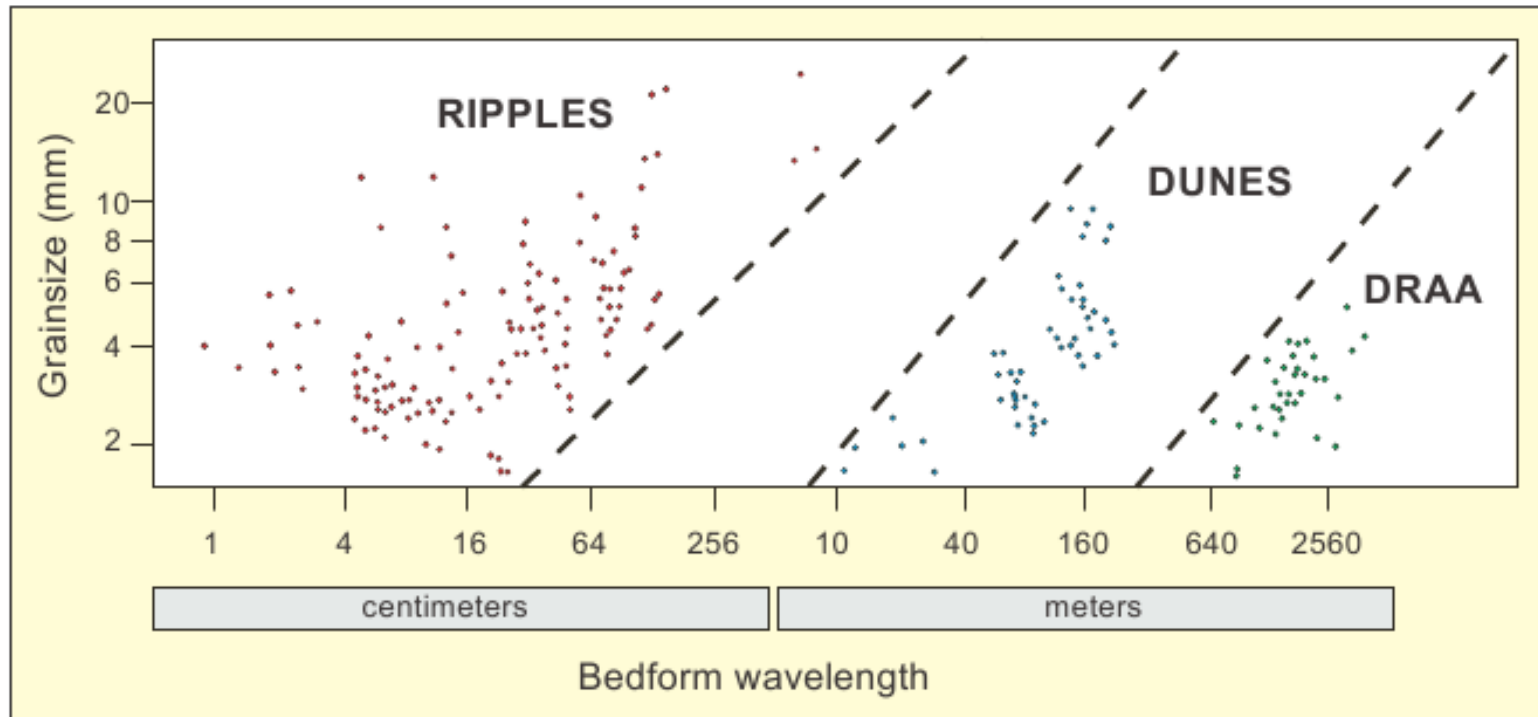


FIG. 7.—Grain size (coarsest twentieth percentile) versus wavelength for eolian bedforms. Note the three distinct groups representing ripples, dunes, and draa. Modified after Wilson (1972).

Mountney (2006)



# Ondulações



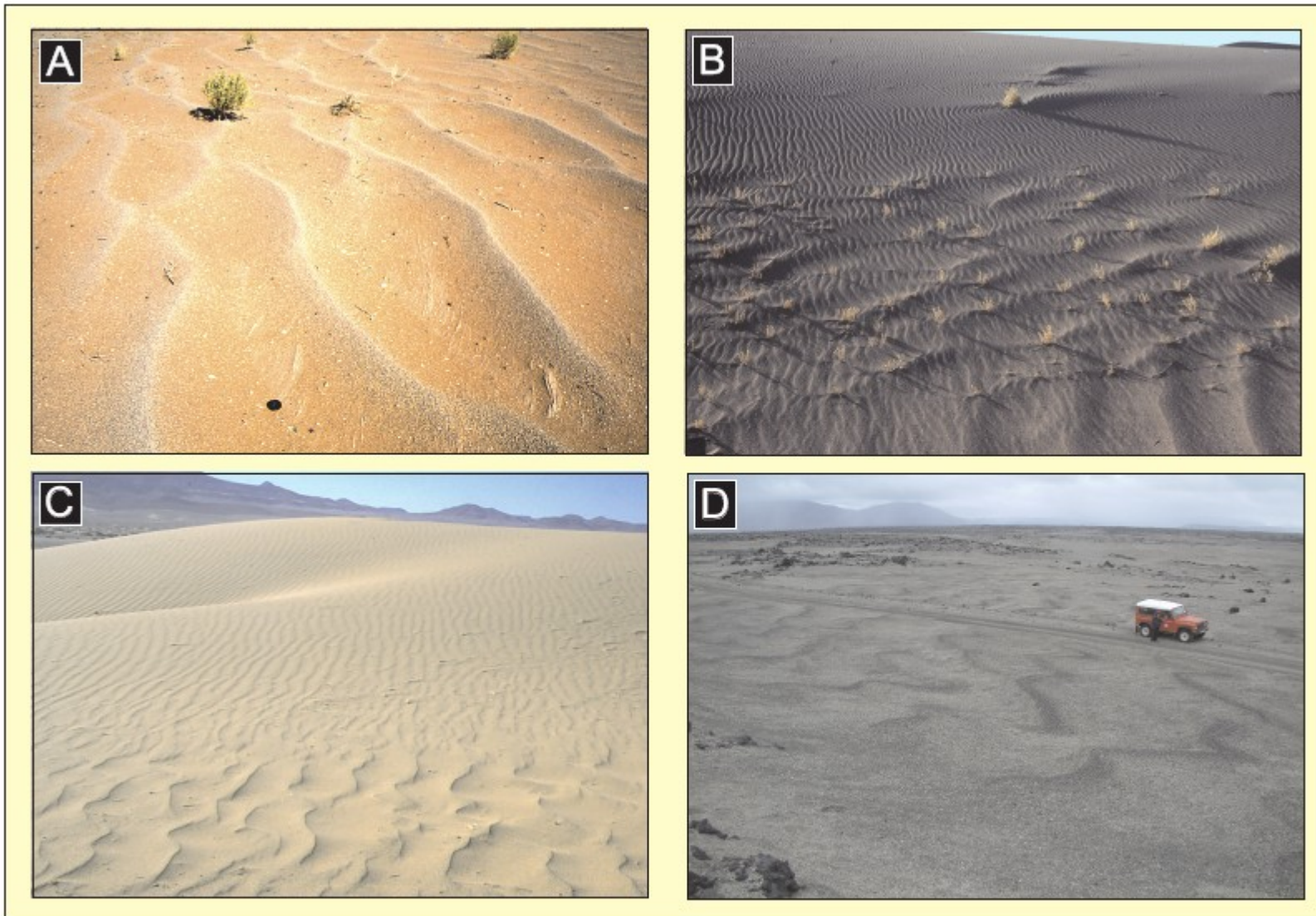


FIG. 8.—Examples of eolian ripple forms. **A)** Sinuous crested with coarser grains on crests. Skeleton Coast, Namibia. **B)** Two scales of superimposed ripples. Idaho (courtesy of John Collinson). **C)** Two scales of ripples developed on the stoss slope of an eolian dune. Huab Basin, Namibia. **D)** Sinuous-crested eolian granule megaripples. Askja sandsheet, central Iceland.

Mountney (2006)

# Draa

## Duna



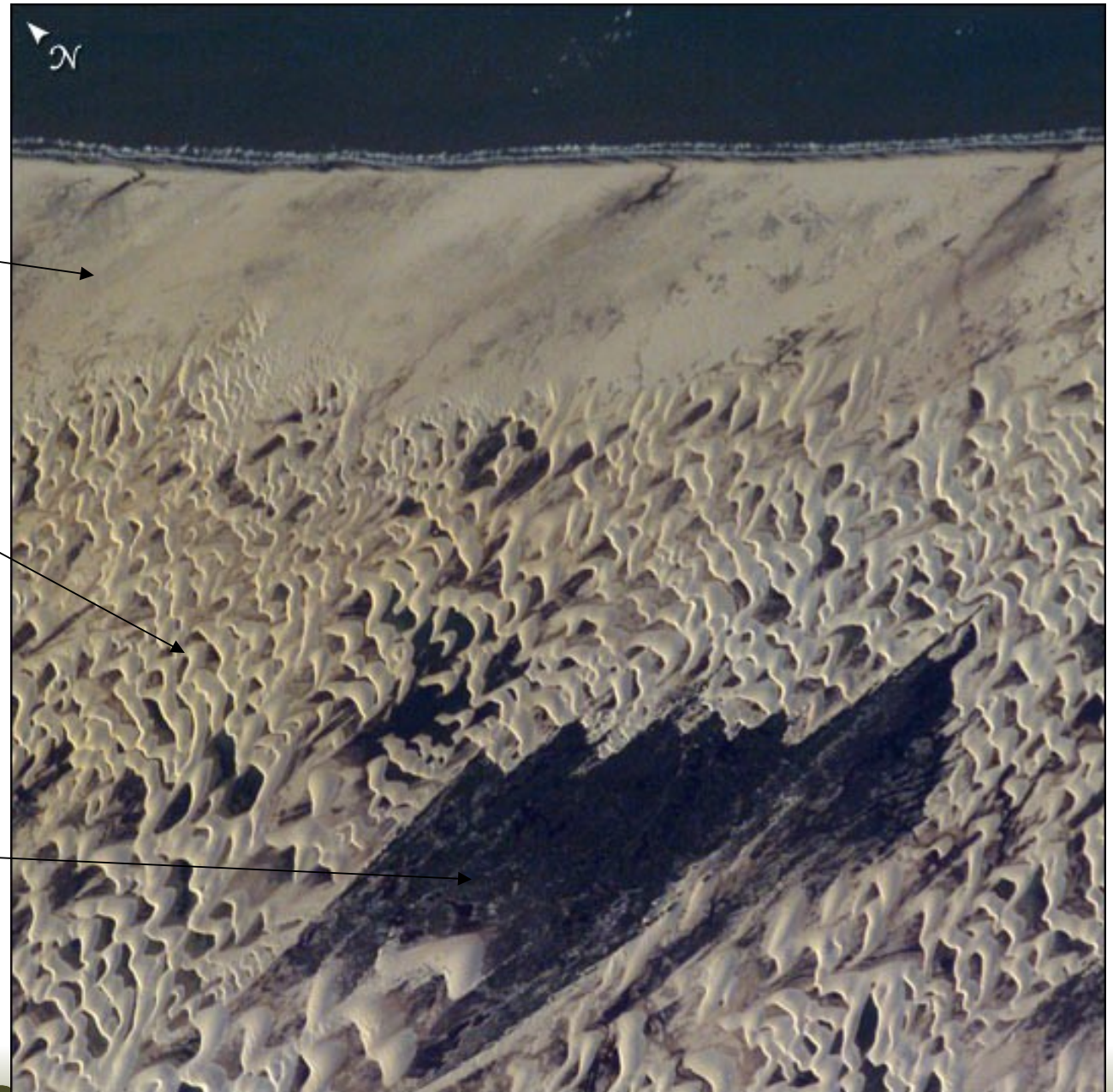
Introdução

Leito

Facies



N



# Lençol de areia



A



Morphology of modern sand sheets. A) Skeleton Coast, northern Namibia. Note dune field in far distance. B) Askja, central Iceland.

Mountney (2006)

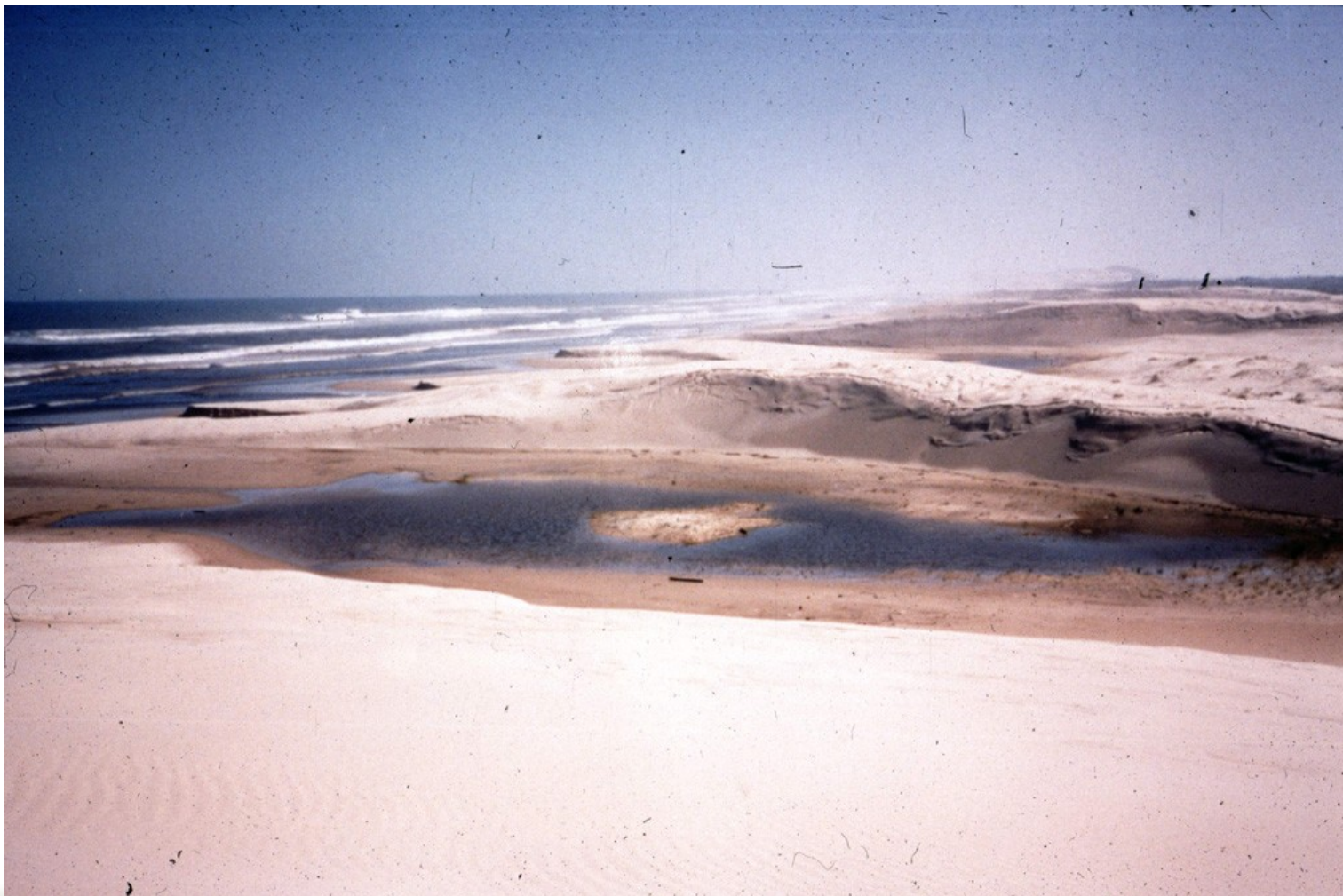
B



# Zonas de deflação



# Depressão interdunar



# Classificação de dunas

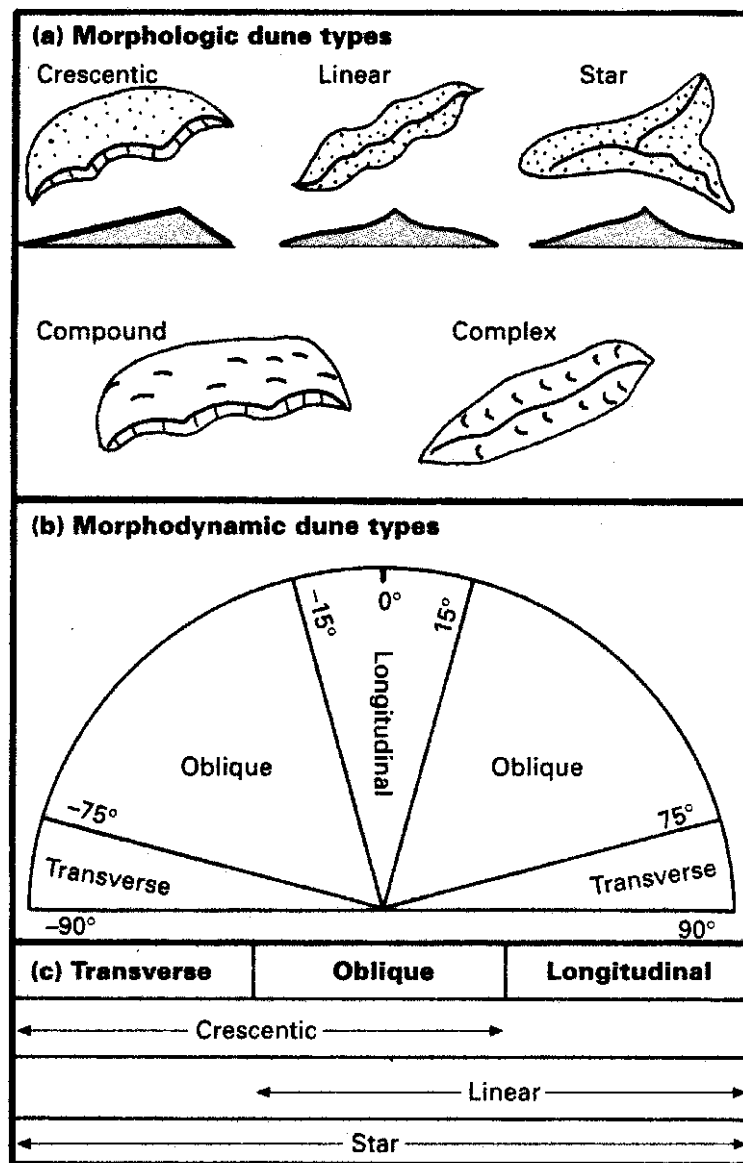
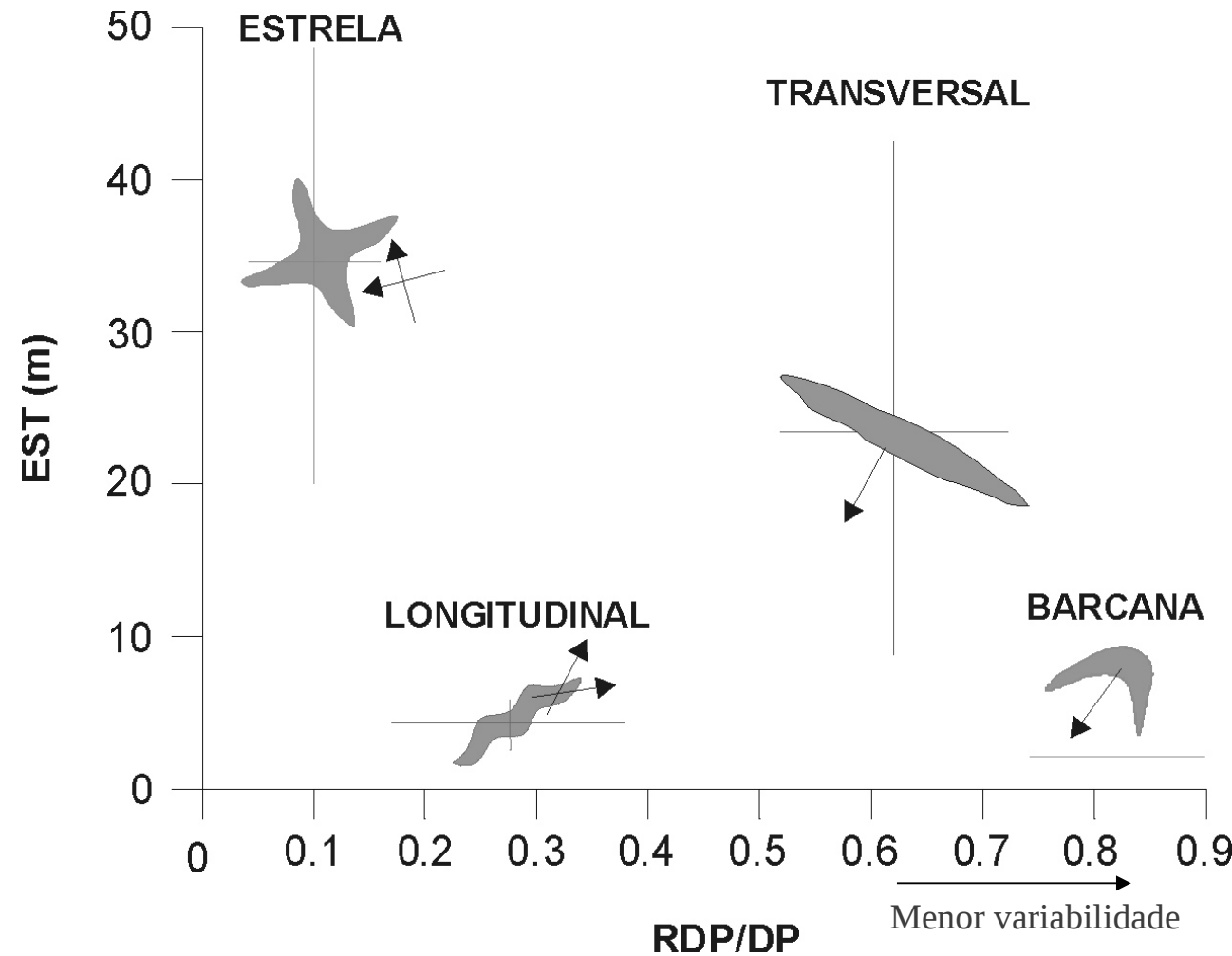


**Figure 5.19** Classification of dunes. (a) Morphological dune types shown in plan view and cross-section for simple dunes, and plan view for compound and complex dunes. (b) Morphodynamic dune types based on orientation of crestline relative to resultant transport direction. (c) Probable range of morphological and morphodynamic dune types (modified from Hunter, Richmond & Alpha, 1983; Kocurek, 1991).

# Dunas livres



RDP/DP = variabilidade do regime de ventos

EST = disponibilidade de areia

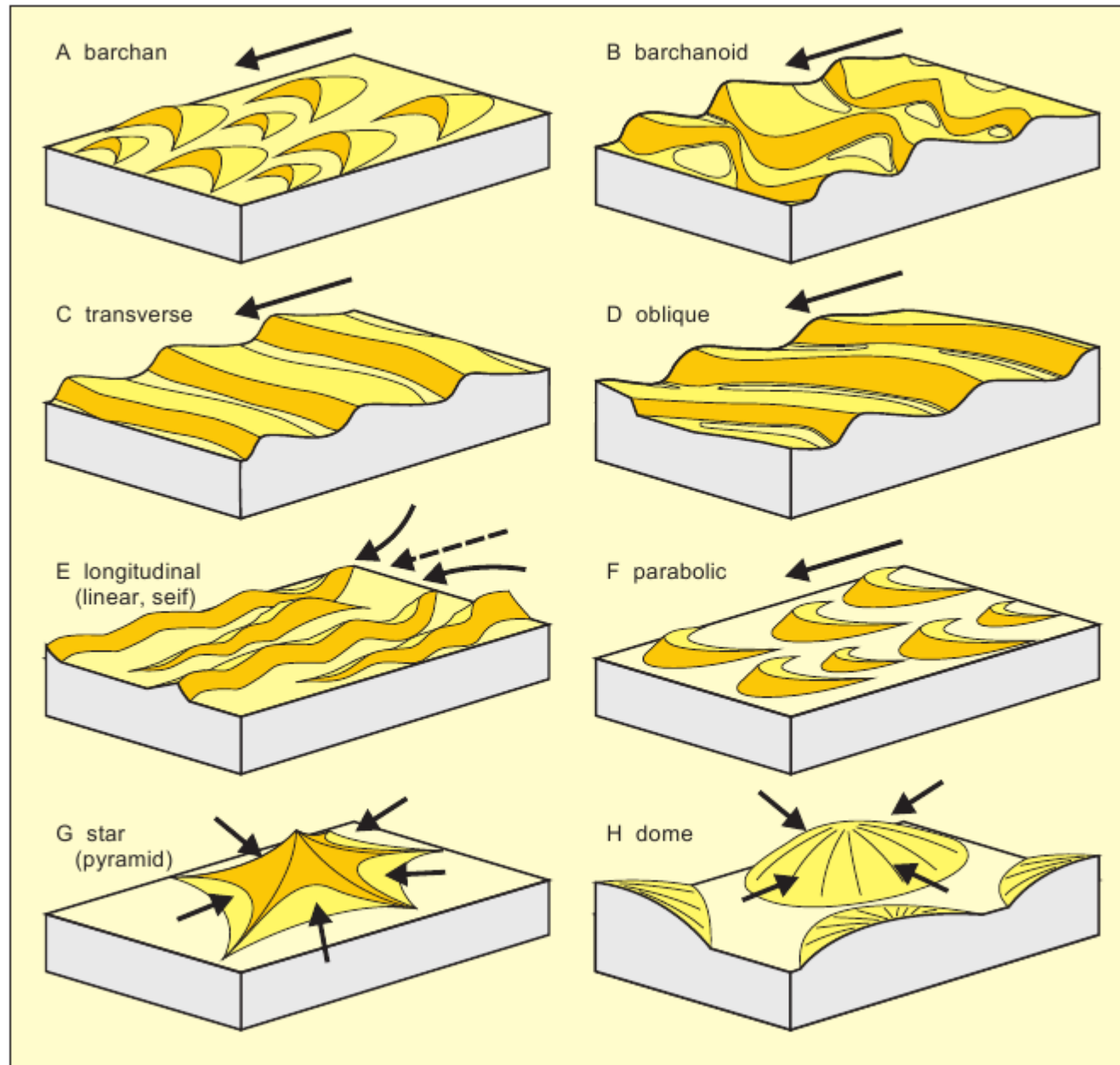


FIG. 10.—Three-dimensional forms of some common dune types. The arrows mark the dominant directions of the effective winds and in case E, the dotted arrow indicates the resultant effective direction.

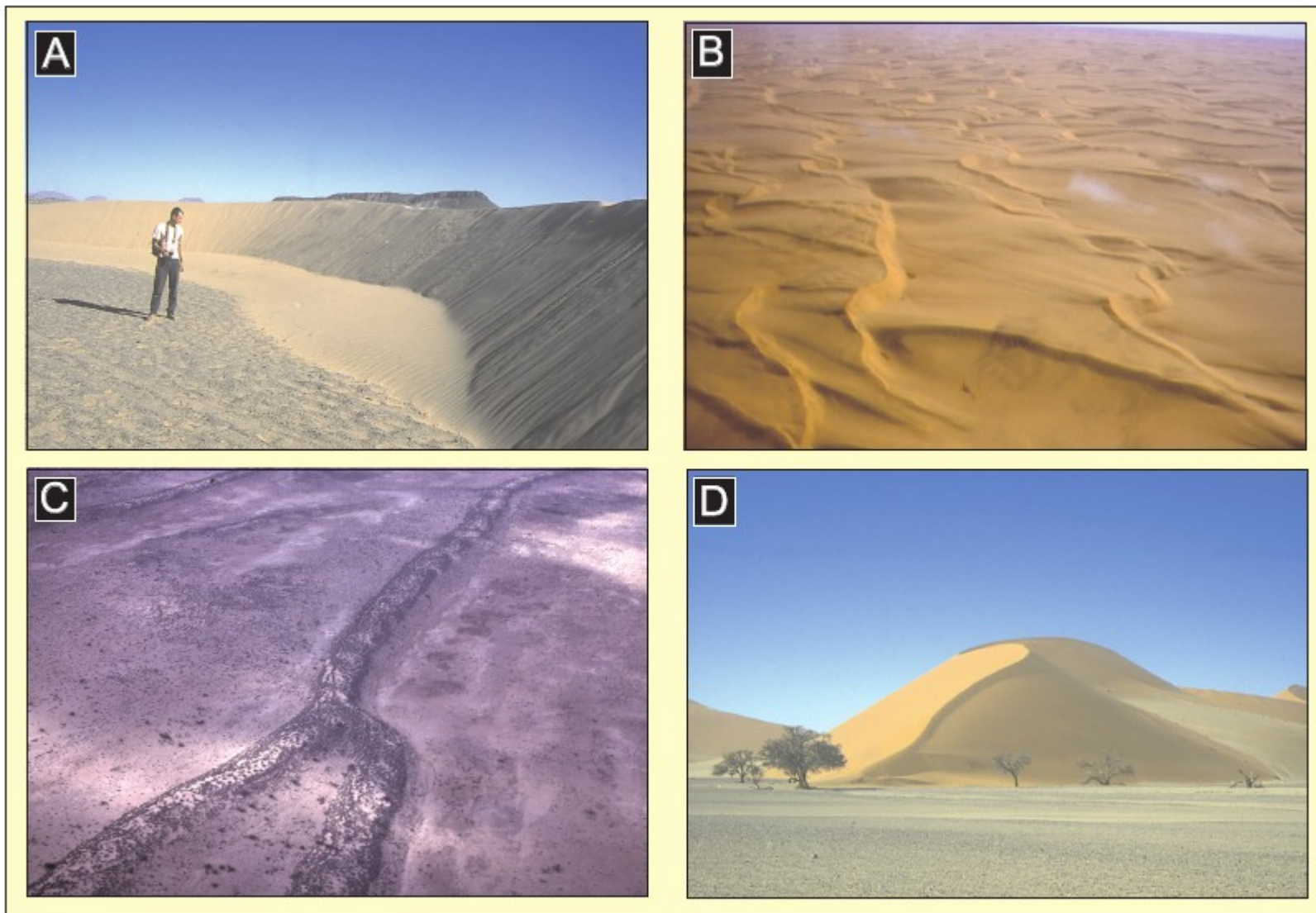


FIG. 11.—Examples of eolian dune forms. **A**) Slipface and plinth of crescentic barchan dune. Skeleton Coast, Namibia. **B**) Transverse dunes. Western Namib Sand Sea. **C**) Linear dune ridge partly stabilized by vegetation. Lake Eyre Basin, Australia (courtesy of John Collinson). **D**) Large star dune, central Namib Sand Sea.

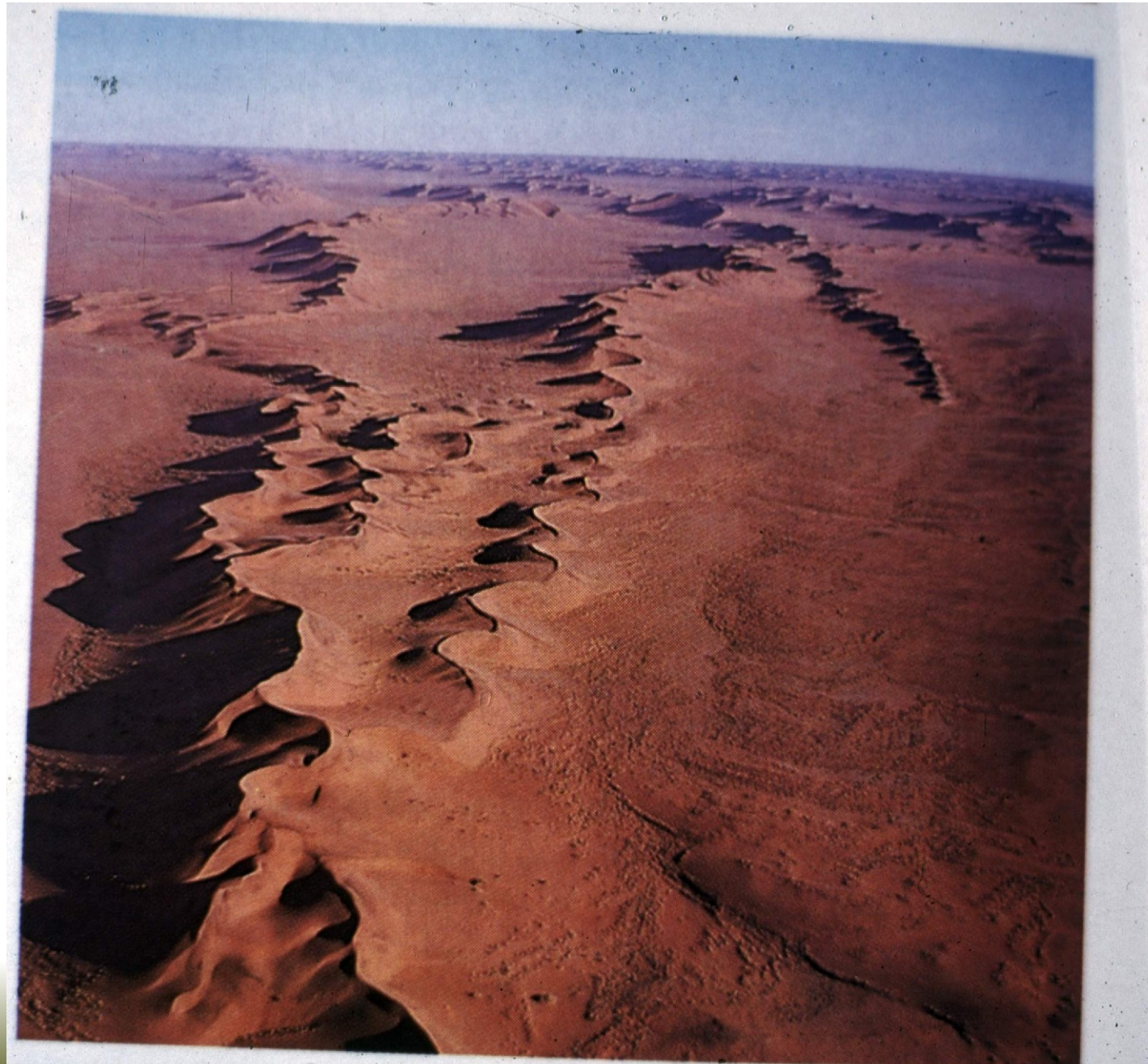
# Dunas barcanas (*crescentic*) e cadeias barcanóides



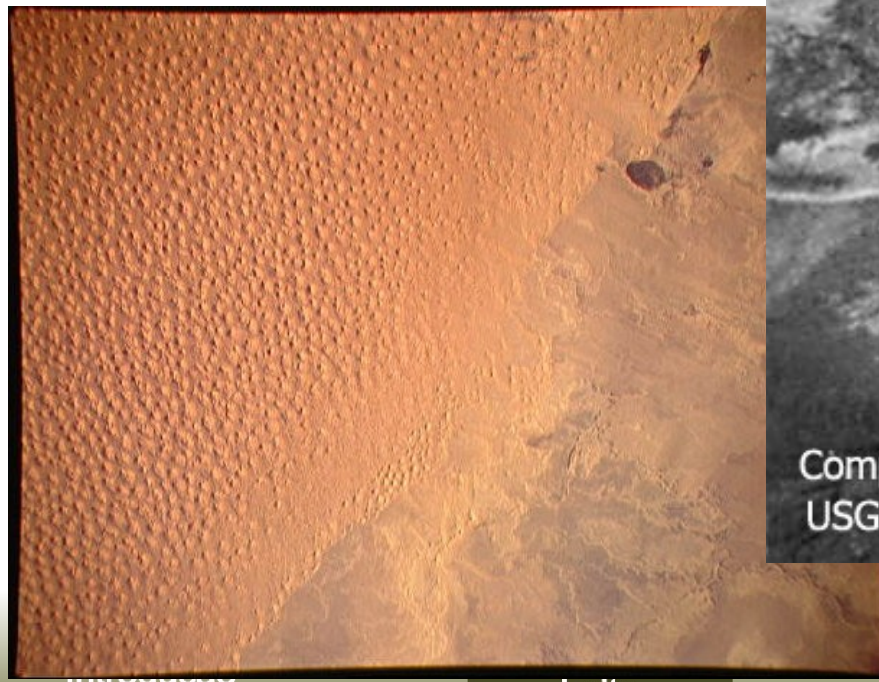
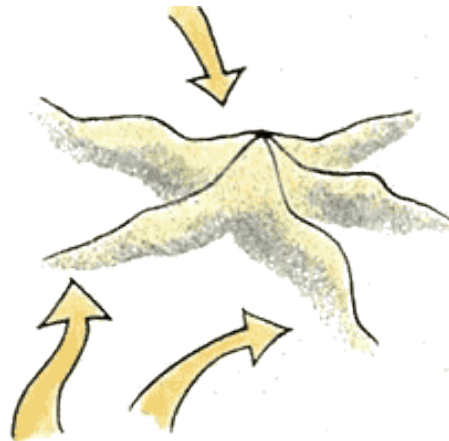
# Dunas transversais



# Dunas longitudinais (*seif*)



# Duna estrela



Leito



Compound Star Dunes of Algeria  
USGS Geomorphology from Space

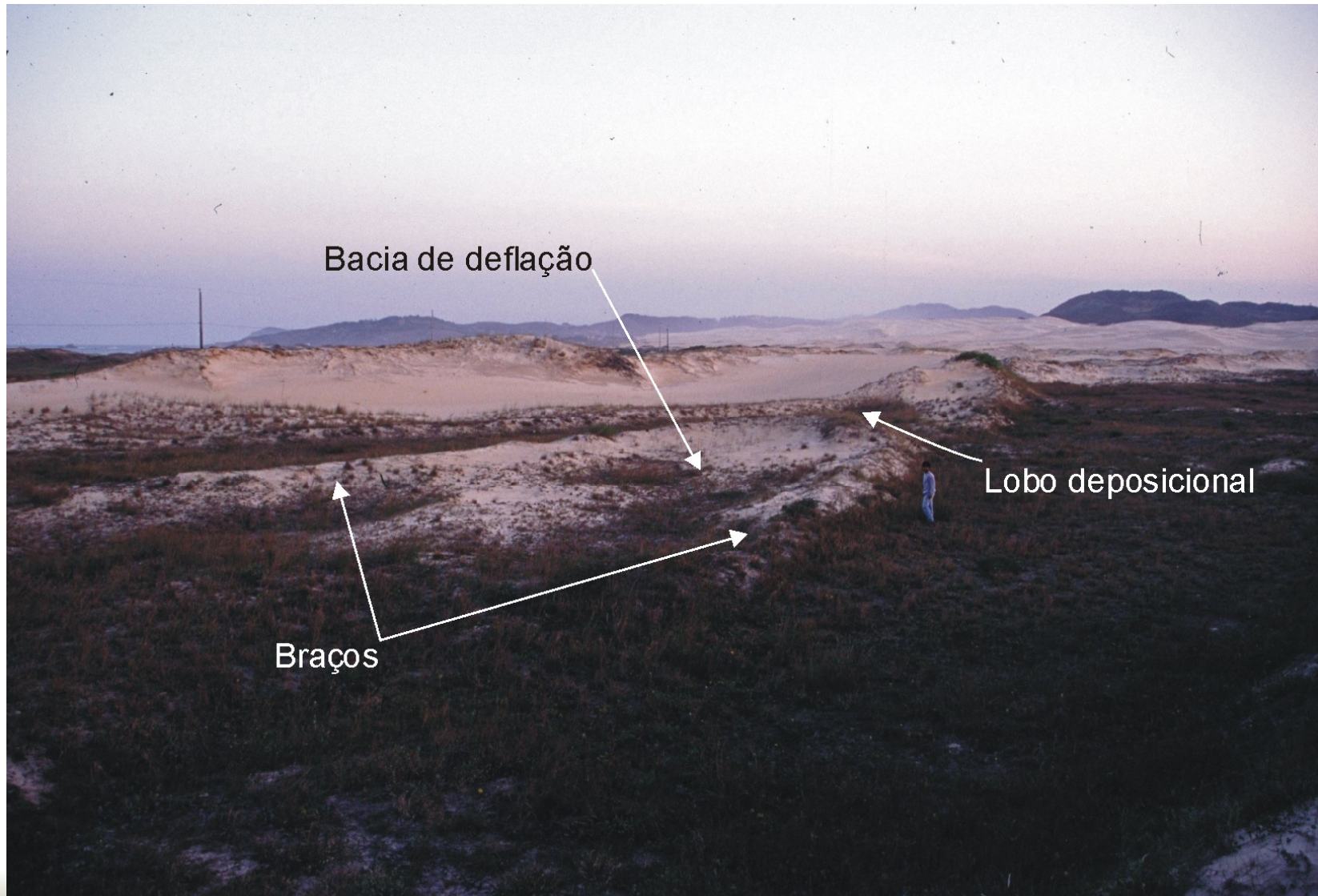
Fácies

Arquitetura

Pré-  
Vegetação

# Dunas vegetadas

# Duna parabólica



# Duna frontal



# Lobos de deflação (blowout)



Dunas livres = aporte sedimentar eólico elevado

Dunas vegetadas = apporte sedimentar eólico reduzido



# Fácies sedimentares

## Estratificação eólica:

- Chuva de grãos (grain fall)
- Fluxo de grãos (grain flow)
- Laminação por migração de marcas onduladas (cruzada e transladante)

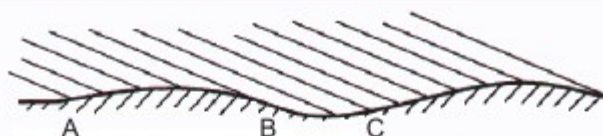
- Laminação cruzada por migração de marca ondulada

- Laminação transladante (*translatent lamination*)

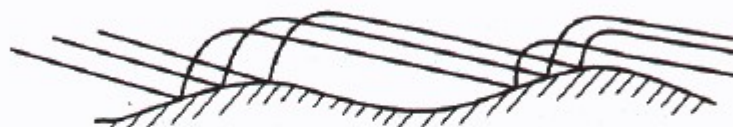
Migração e cavalgamento de marcas onduladas

Marcada por variação granulométrica da crista para o pé da m.o. (ressalta apenas os planos de cavalgamento em baixo ângulo)

Raramente há também cruzadas de estratos fontrais da m.o.

**A**

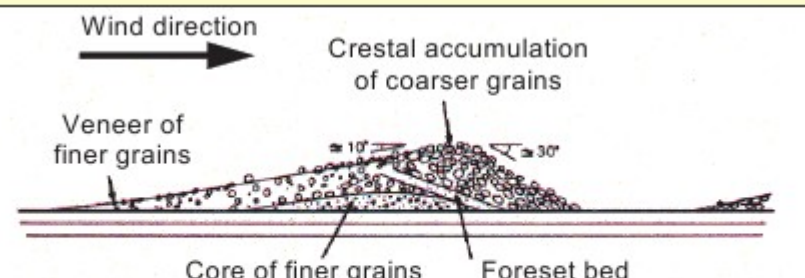
Variation in impact intensity over perturbation in bed.  
Note higher intensity in AB compared to BC



Ripple spacing is controlled by saltation path length, which  
is itself primarily a function of grain size and wind velocity.



Alternation of impact and shadow zones on developing  
wind ripple (after Anderson, 1987).

**B**

Laminae and grain size distribution within eolian ripples (after Sharp, 1963).

Grãos maiores estacionam na zona de impacto  
e sofrem arrasto para a crista até decolarem  
novamente.

Grãos menores ficam aprisionados na zona  
de sombra e não param na zona de impacto.

FIG. 9.—Generation of eolian ripples. **A**) Model for the generation of saltation ripples. After Anderson (1987). **B**) Grain texture in eolian ripples. After Sharp (1963).

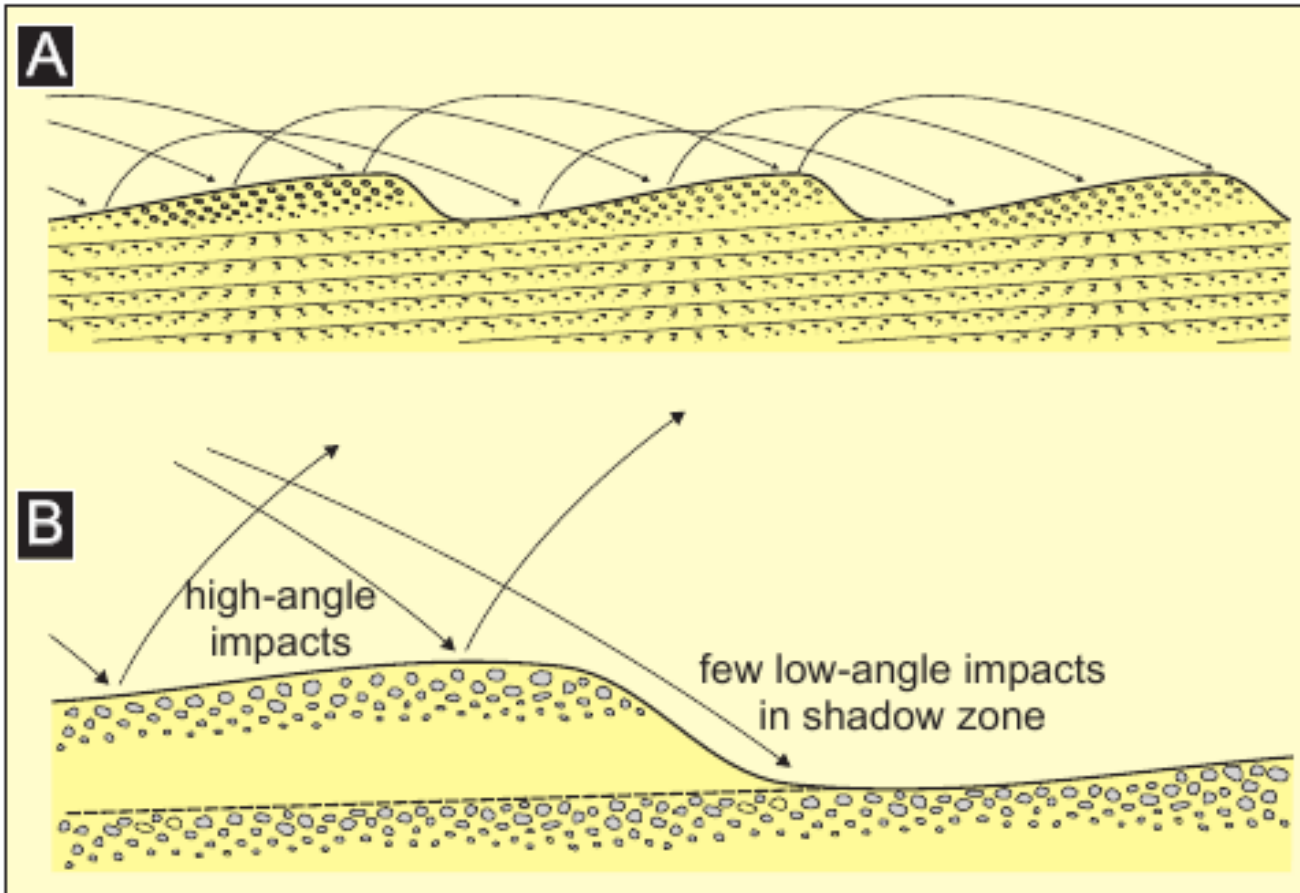
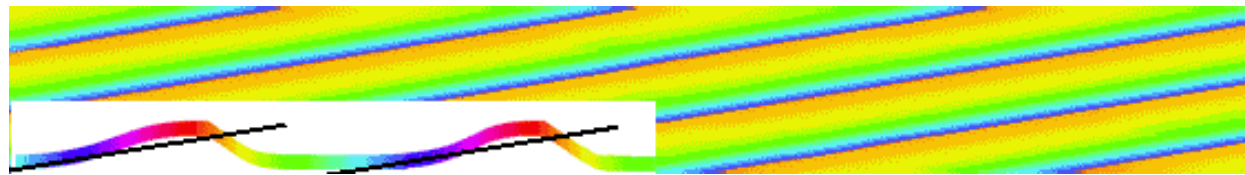


FIG. 17.—Wind ripples generated by ballistic impact of grains. The ripple spacing relates in a general way to the saltation path length, which is the characteristic distance that individual grains hop downwind as a result of grain collision on the bed. The saltation path length is a function of grain size, shape and density, and mean wind velocity and gustiness close to the bed. **A)** The migration of wind ripples generates subparallel lamination. **B)** The impact angle of saltating sand grains differs between stoss sides and lee slopes. High-angle impacts on the stoss of the bedforms promotes creep of coarser grains towards the ripple crest. Downwind-facing lee slopes form a shadow zone where relatively few low-angle impacts occur, thus encouraging the accumulation of finer grains in ripple troughs. As ripples migrate downwind, this sorting mechanism generates lamination with inverse grading.

# Laminação transladante



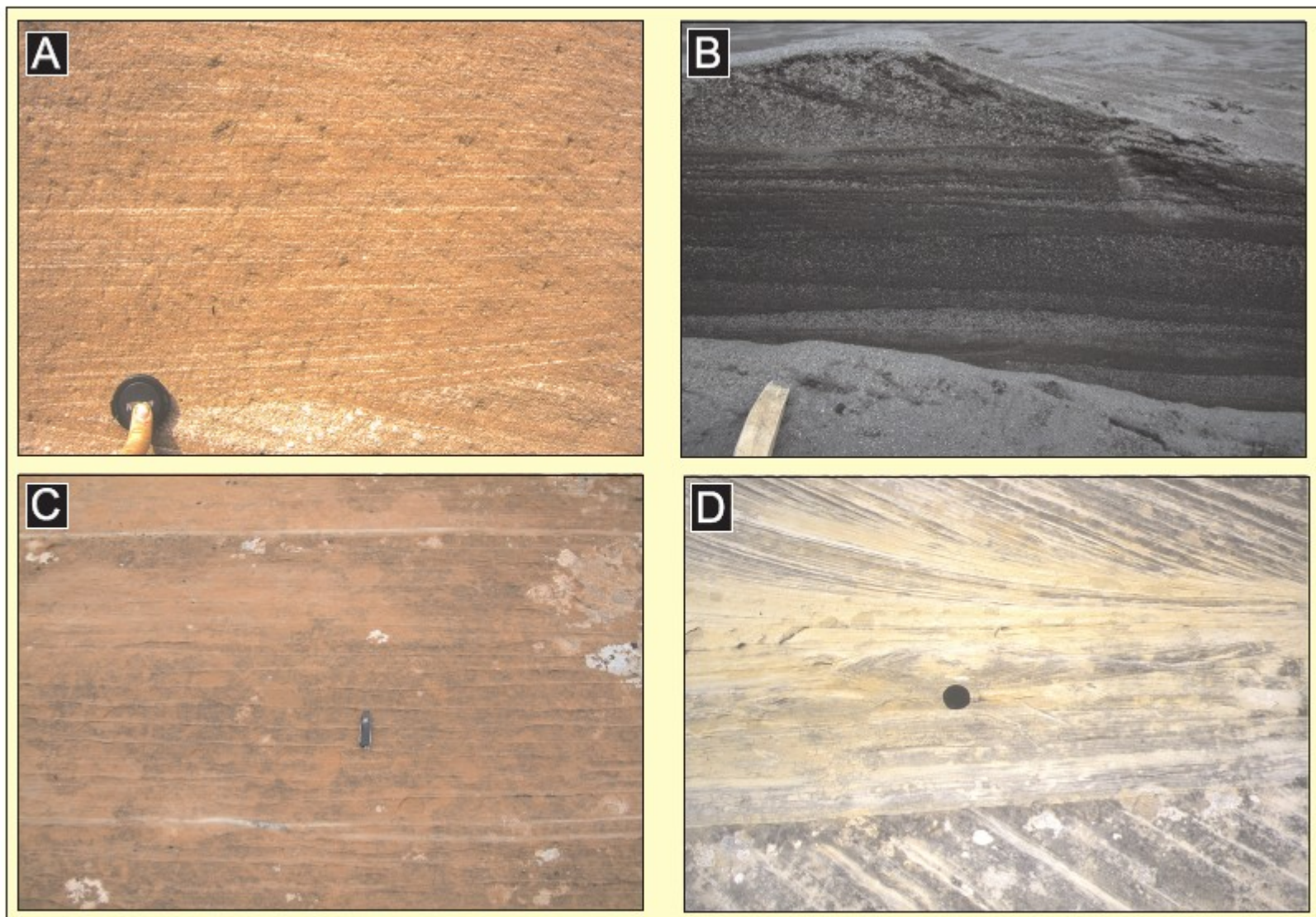


FIG. 15.—Examples of eolian ripple internal stratification. **A**) Pinstripe lamination, Etjo Formation, Cretaceous, Namibia. **B**) Inversely graded translatent strata, Askja, Iceland. **C**) Sharply defined wind ripple laminae interbedded with thin grainfall laminae. Lower Cutler Beds, Pennsylvanian–Permian, Utah, U.S.A. **D**) Wind-ripple strata on a dune plinth. Cedar Mesa Sandstone, Permian, Utah, U.S.A.

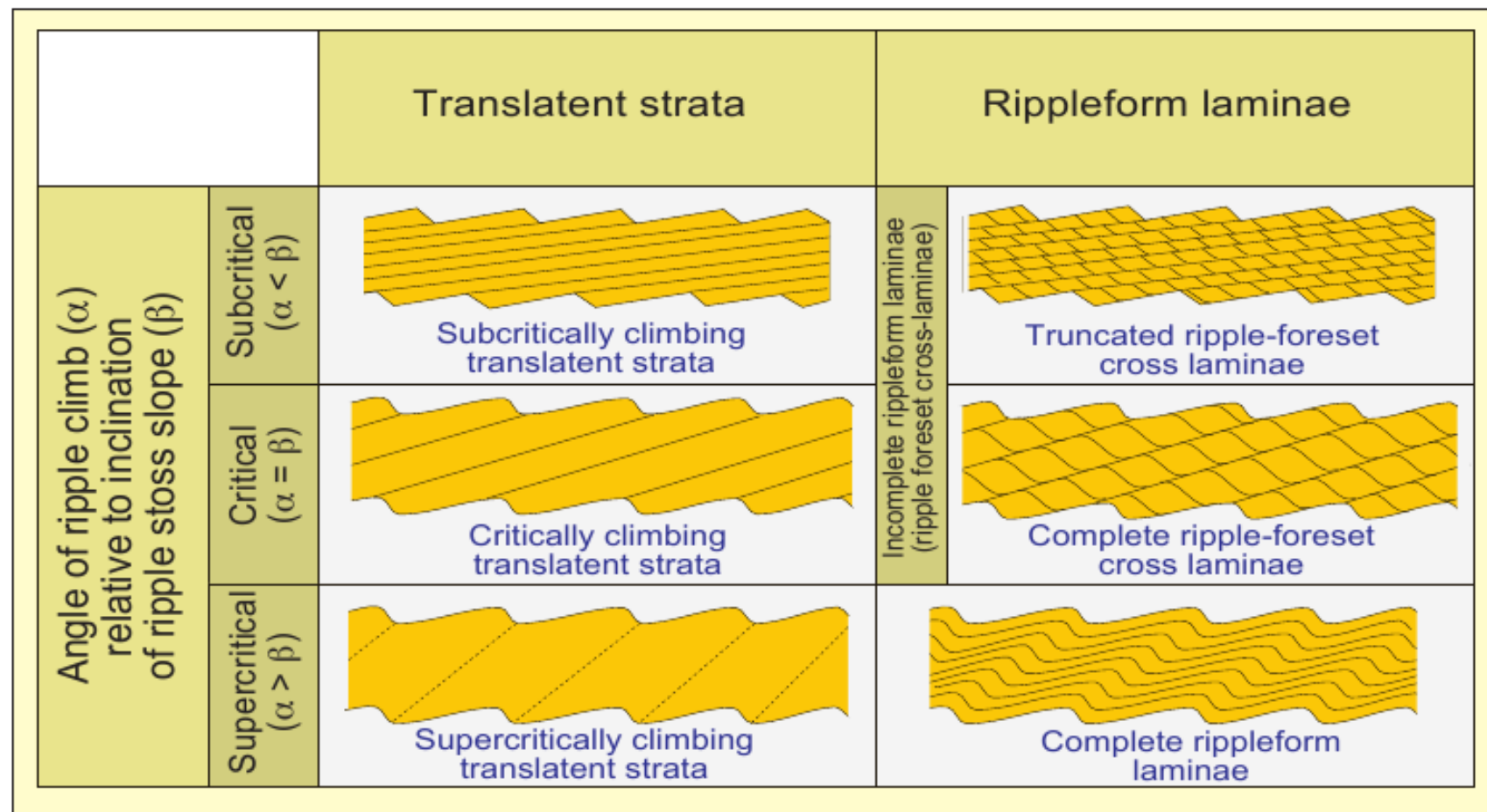
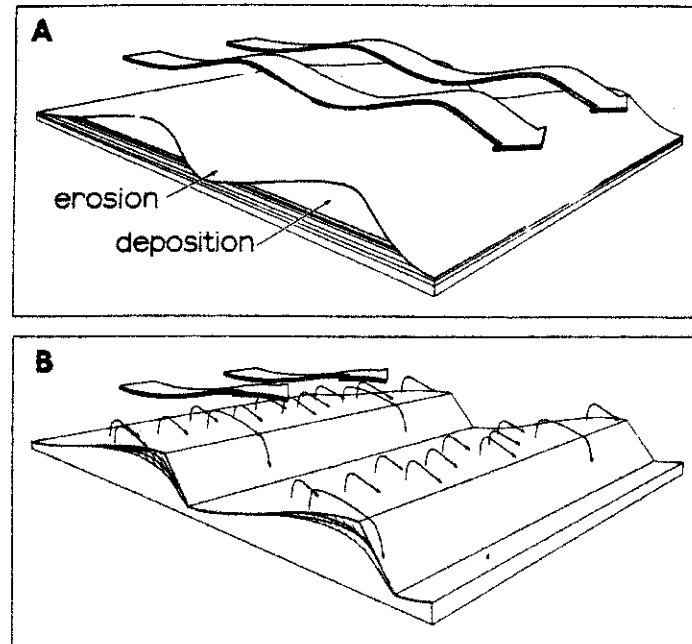
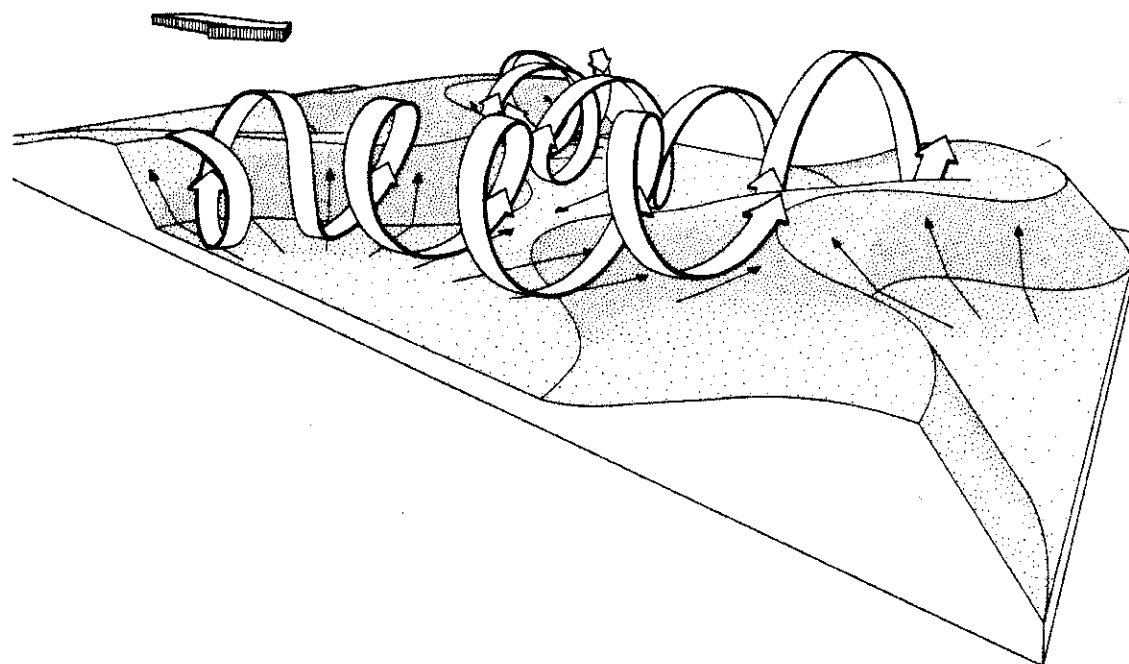


FIG. 16.—Classification of wind-ripple stratification types according to angle of ripple climb relative to the inclination of the stoss slope of the bedform and the presence or absence of cross-lamination. Modified after Hunter (1977).



**Figure 16.10** The hypothetical first two stages of transverse dune formation: A. wavelike pattern in the wind erodes and deposits alternate ridges and hollows; B. slipfaces develop.

Source: Warren, 1979, figure 10.10, p. 337.



**Figure 16.11** Horizontal vortex eddies associated with a barchanoid transverse dune which propagate downwind distortions in the subsequent ridge.

Source: Warren, 1979, figure 10.12, p. 340.

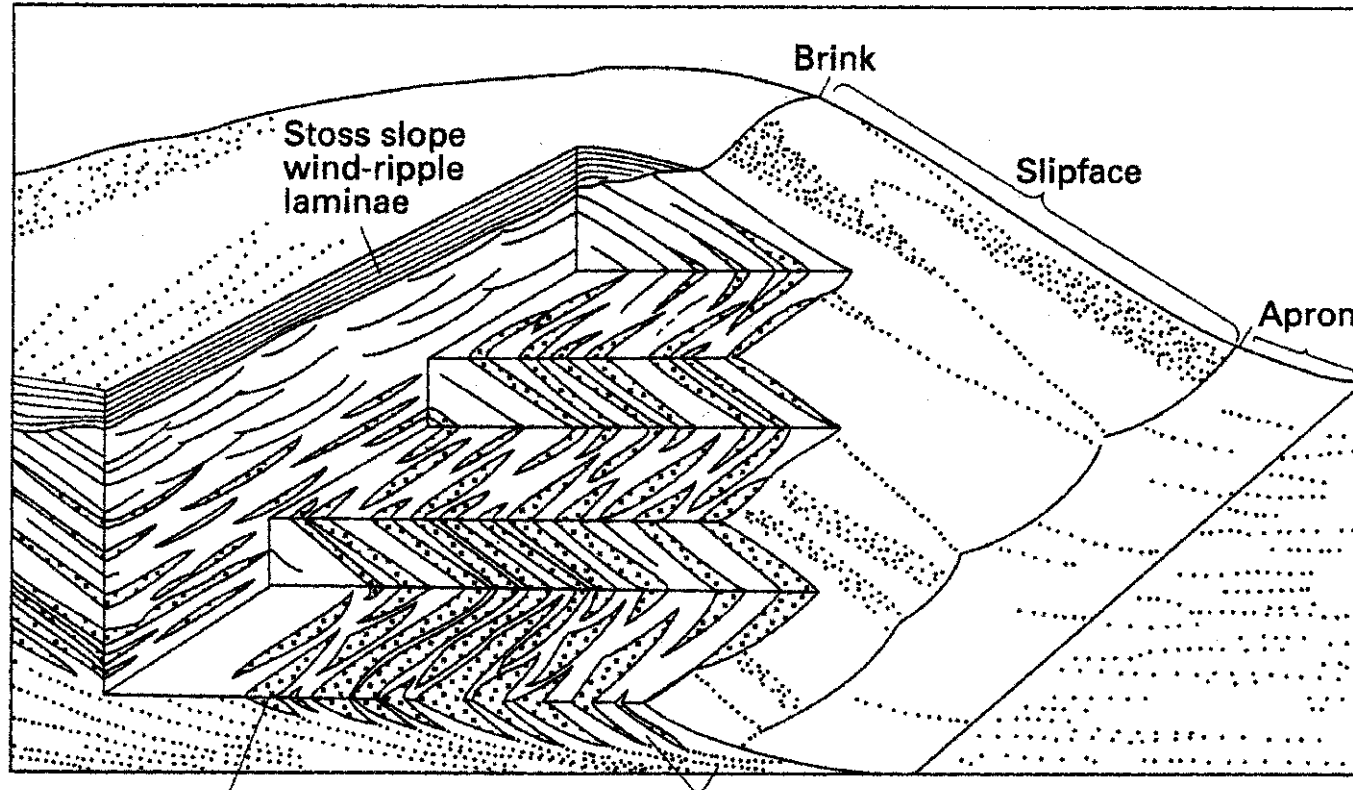


**Figure 5.3** ‘Small’ transverse dune, with slipface and basal apron, showing horizontal and cross-sections with stratification (from Hunter, 1977a).

# Fluxo de grãos

Lentes mais espessas no pé da duna

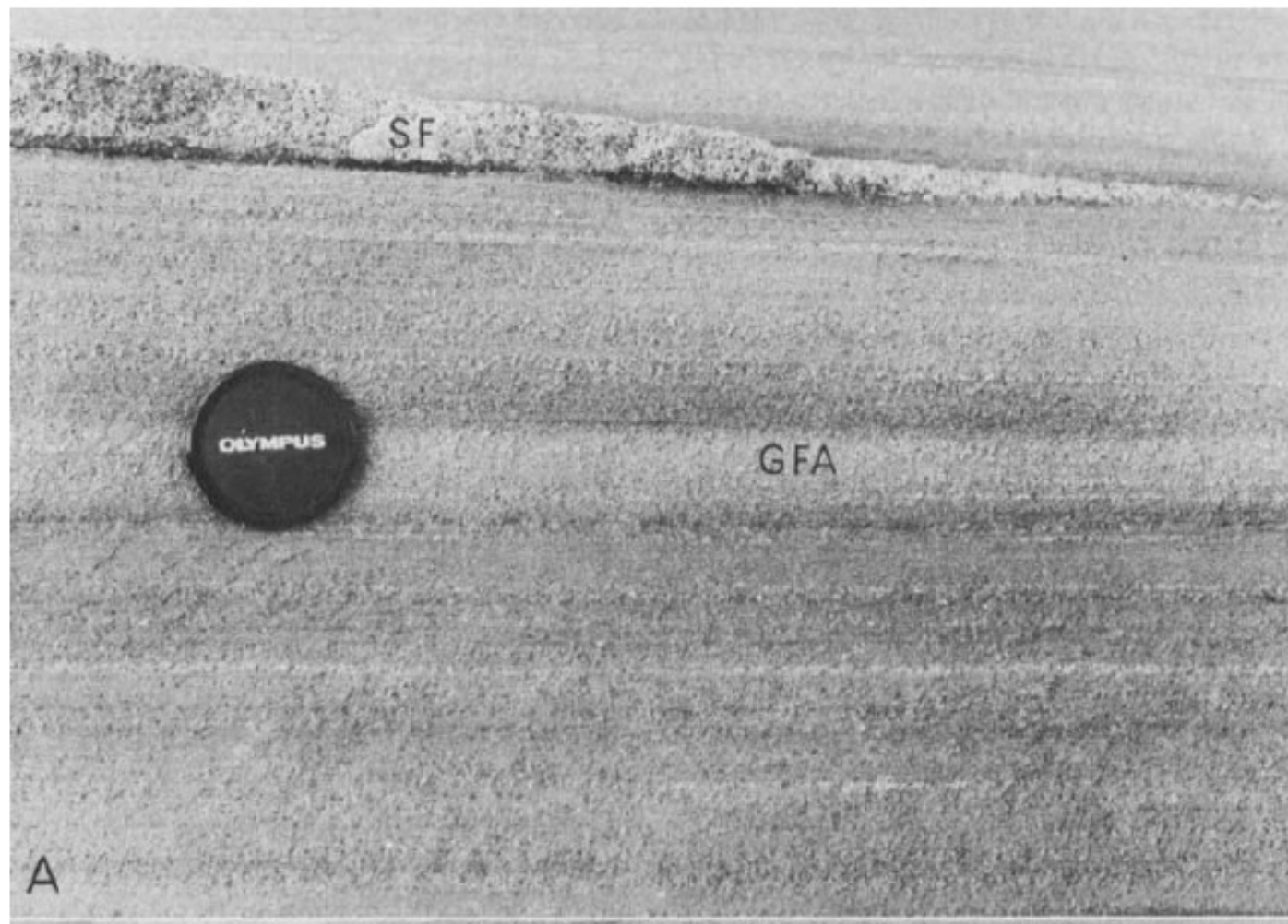
Empacotamento aberto

Gradação inversa

Espessura de centímetros

# Fluxo de grãos





Clemmensen & Abrahamsen (1983)



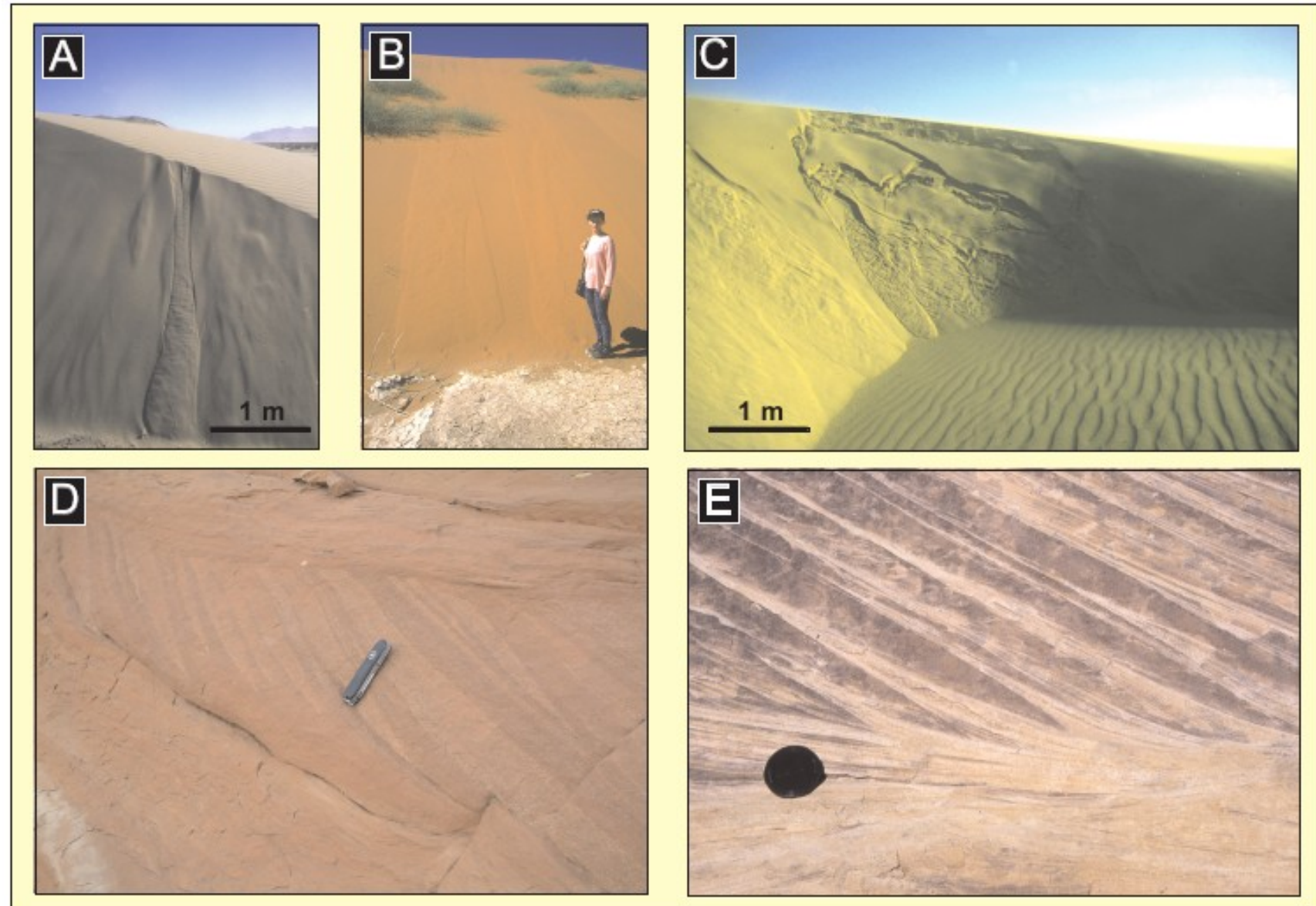


FIG. 18.—Examples of eolian grainflows and the characteristic strata that they produce. **A)** Scarp-recession grainflow, Namibia. **B)** Slump-degradation grainflows, Namibia. **C)** Slab slide failure degenerates downslope into a slump-degradation grainflow, Namibia. **D)** and **E)** Grainflow tongues pinching out into wind-ripple strata. Cedar Mesa Sandstone, Permian, Utah, U.S.A.

# Chuva de grãos

Repouso da areia em saltação

Laminação fina inclinada na frente da duna

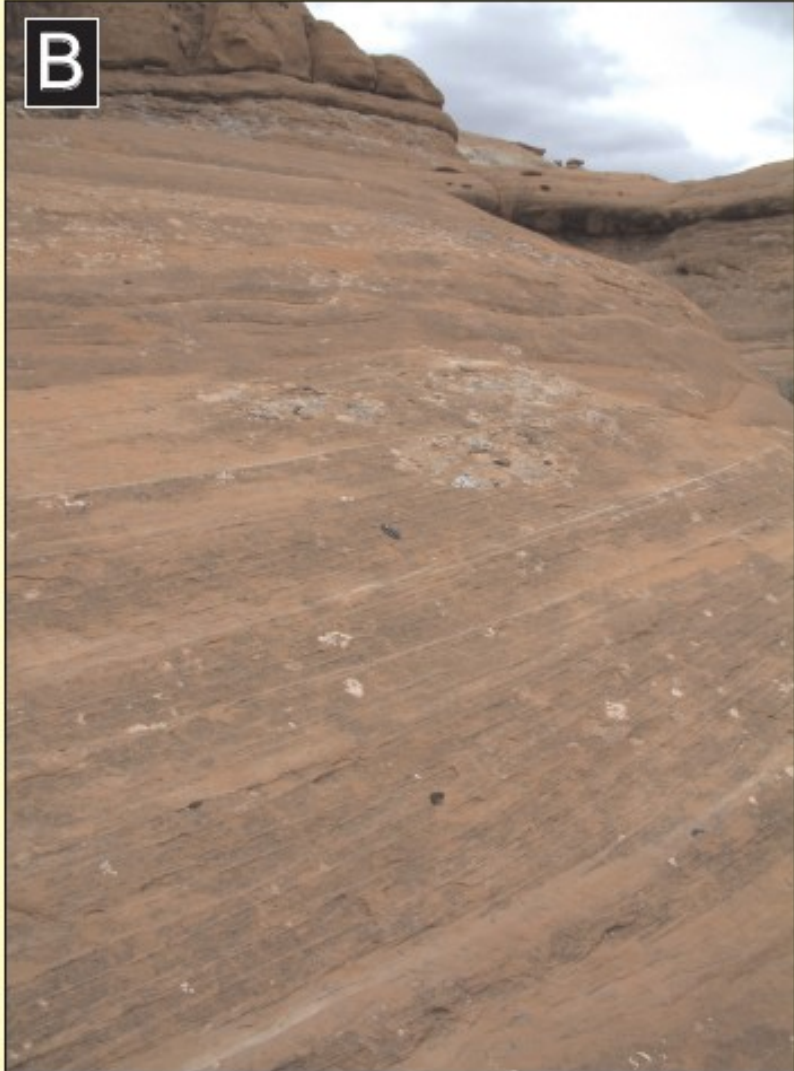


FIG. 19.—Examples of eolian grainfall and the characteristic strata that it produces. **A**) Saltation of sand-size particles over the brink of a dune to form a suspension cloud. Deceleration of the airflow in the lee-side depression results in a loss of carrying capacity, and the grains fall onto the upper part of the lee slope as grainfall deposits. Kalahari Desert. **B**) Grainfall facies interbedded with wind-ripple strata. Individual grainfall units rarely exceed 5 mm in thickness but tend to be laterally continuous along the strike of the cross-bedding for several meters to tens of meters. Interbedded units of wind-ripple strata are thicker (1–2 cm). Cedar Mesa Sandstone, Permian, Utah, U.S.A. Penknife for scale.

# Fácies de dunas

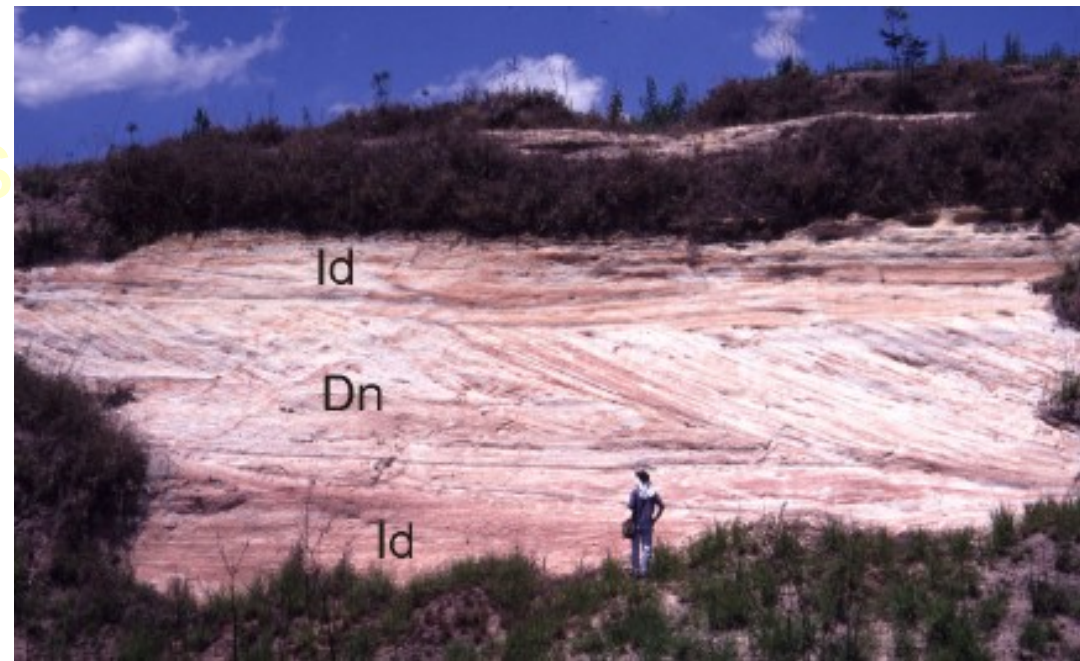


Fácie



vegetação

# Fácies de interdunas



Leito

Fácies

Arquitetura

Pré-Vegetação

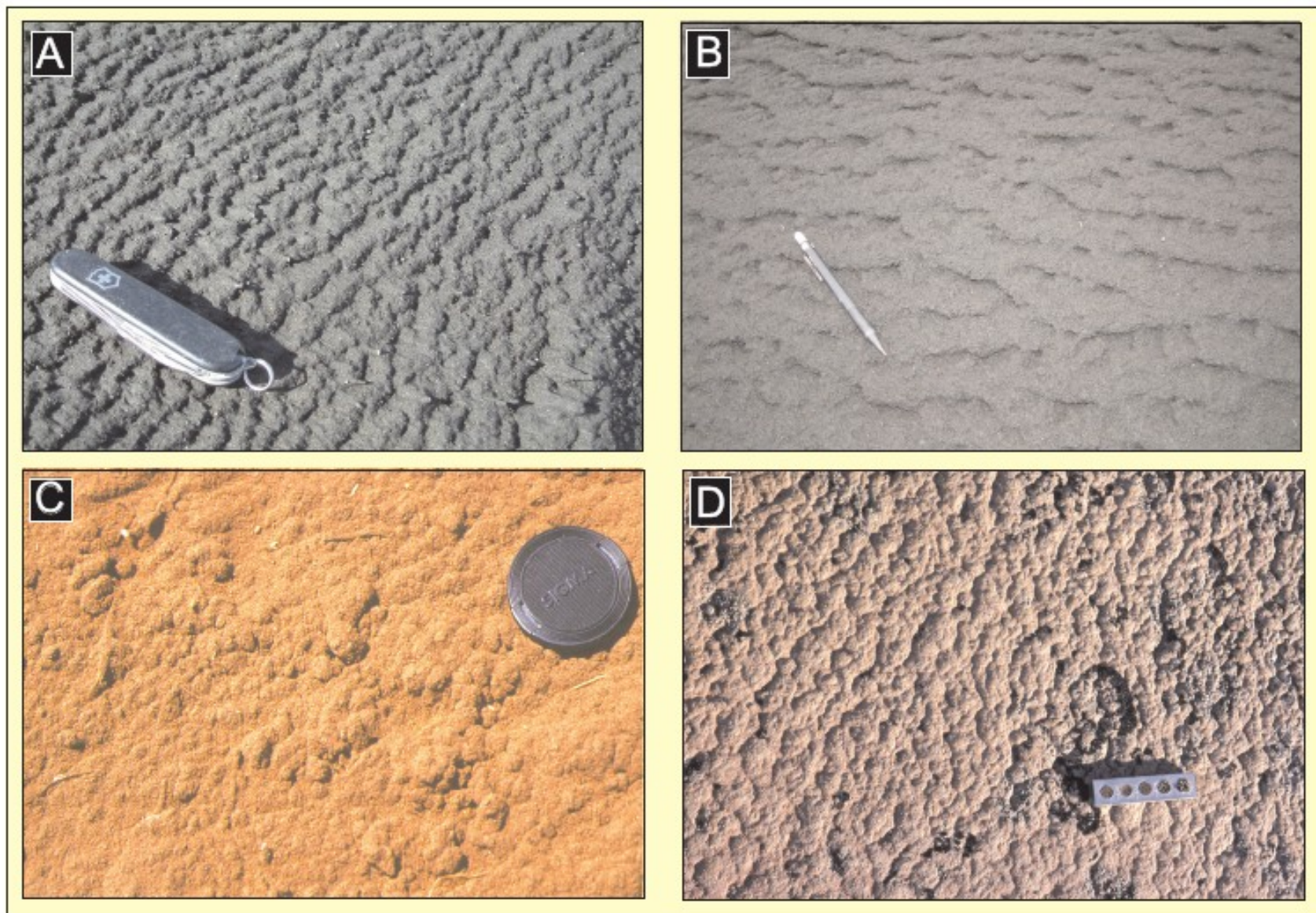


FIG. 20.—Examples of eolian adhesion ripples. A) Sólheimasandur, southern Iceland. Accretion occurs on the steeper upwind-facing slopes, and the “ripples” migrate upwind over time. B) Askja, central Iceland. C) Adhesion warts, Mojave desert. D) Adhesion structures on a bedding surface, Precambrian, Greenland (courtesy of John Collinson).

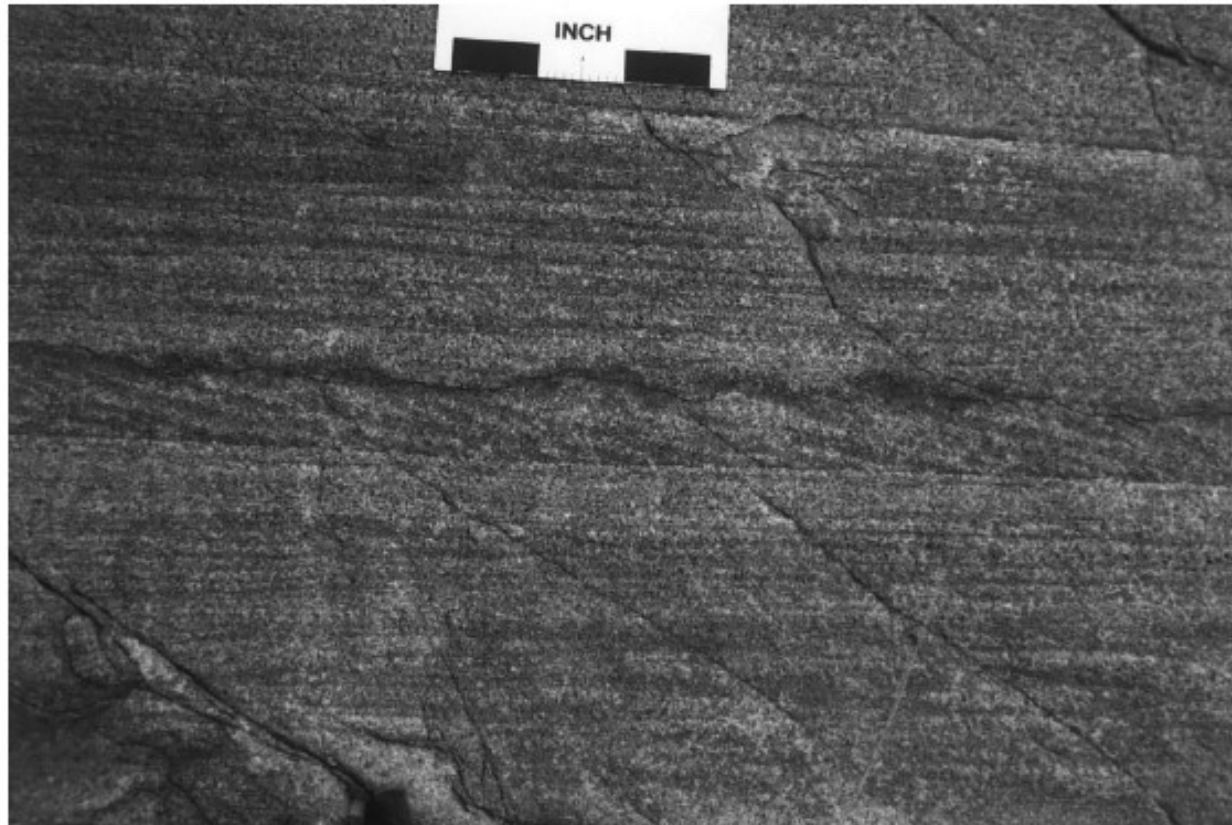


Fig. 5. Adhesion ripple cross-stratification from the Whitworth Formation, Mount Isa Orogen, Australia, representing dune-plinth, sand-sheet or interdune deposits.

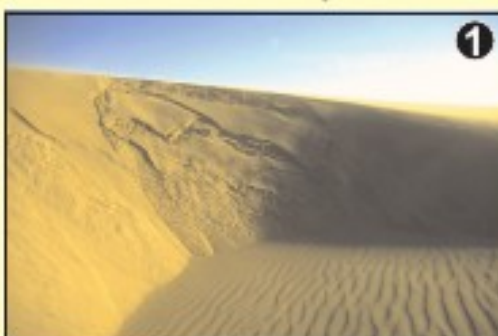
Eriksson & Simpson (1998)



Fig. 7. Adhesion ripples/warts from the Upper Mount Guide Quartzite, Mount Isa Inlier, Australia, preserved in a sand-sheet deposit.

Eriksson & Simpson (1998)

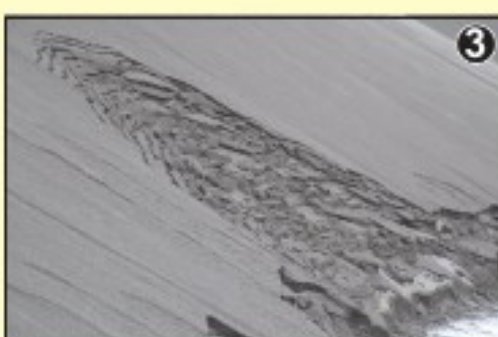
## Modern examples



Slipface on barchan dune with grainflow avalanches. Wind ripples in dry interdune. Skeleton Coast, Namibia.

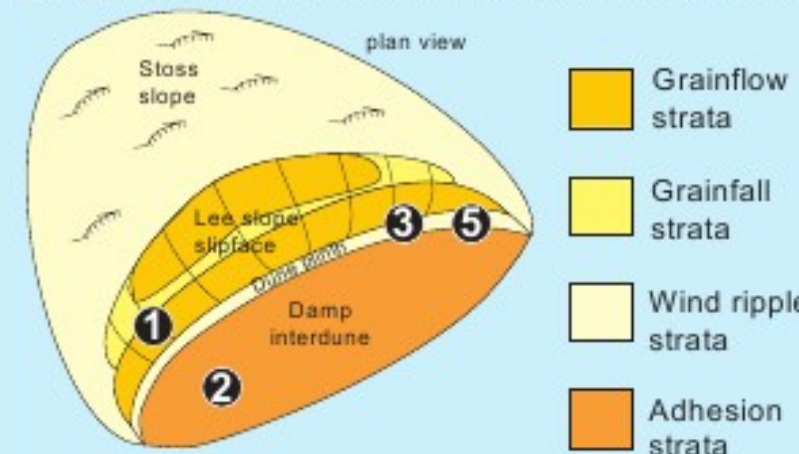


Adhesion structures on a damp interdune surface. Plan view. Monument Valley, northern Arizona.

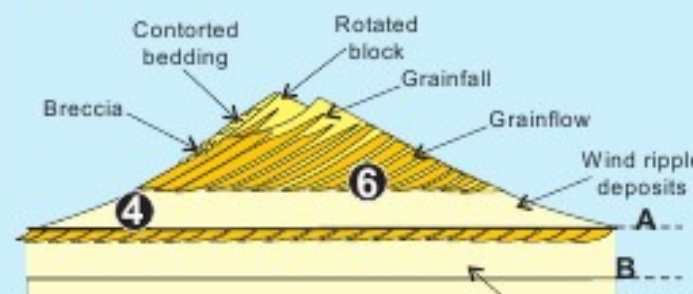


Slipface collapse due to cohesive slab slide. Slabs of wet sand fail without loss of internal structure. Askja region, NE Iceland.

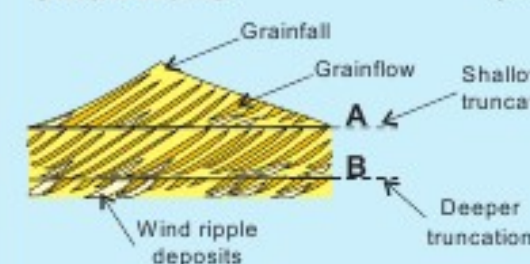
## Eolian facies distribution on crescentic dunes



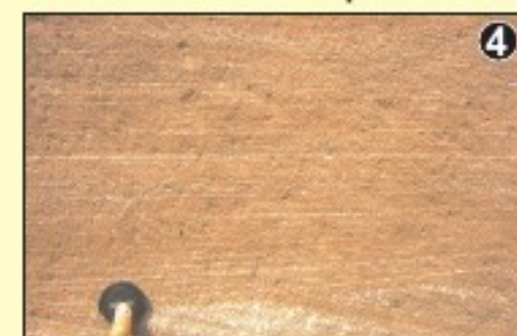
## Large Dune



## Small Dune



## Ancient examples



Wind ripple strata in section displaying characteristic pinstripe lamination. Etjo Formation, NE Namibia.



Wavy laminae in damp interdune unit passing up into overlying wind ripple dune plinth strata. Helsby Sandstone, UK.



Grainflow tongues merging with wind ripple strata that represent dune plinth deposits. Cedar Mesa Sandstone, Utah.

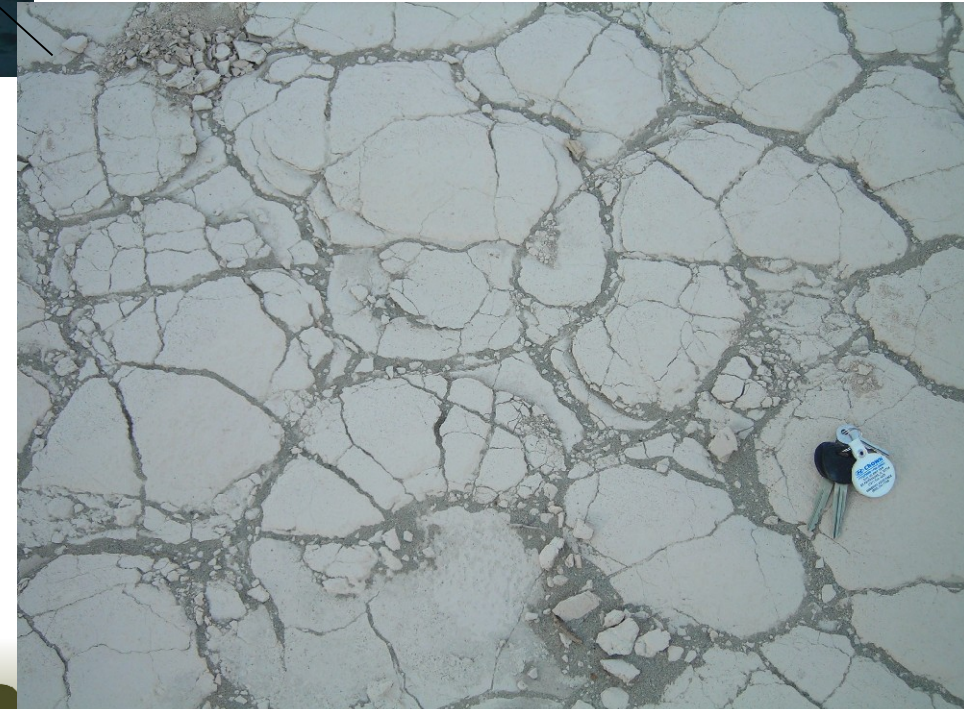
FIG. 21.—Examples of characteristic eolian facies and their distribution on a simple crescentic (barchan) dune and on large-scale and small-scale eolian dunes truncated to different levels (A, B). Level of truncation influences the preservation of facies types in the geological record, with features characteristic of the upper slipface lost. Modified after Kocurek and Dott (1981).



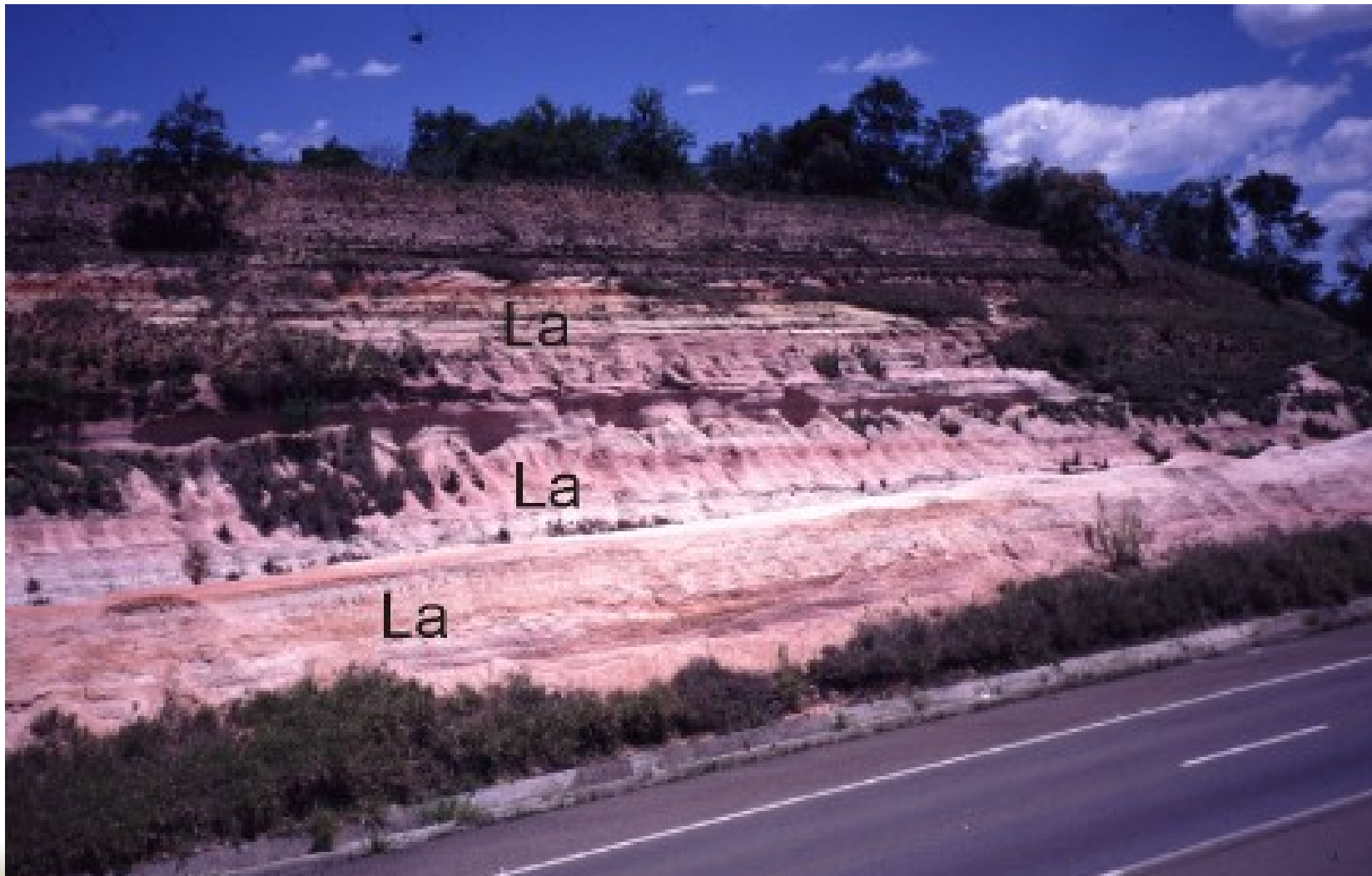
Interação eólico-fluvial

# Depressão interdunar

Gretas de contração



# Lençol de areia



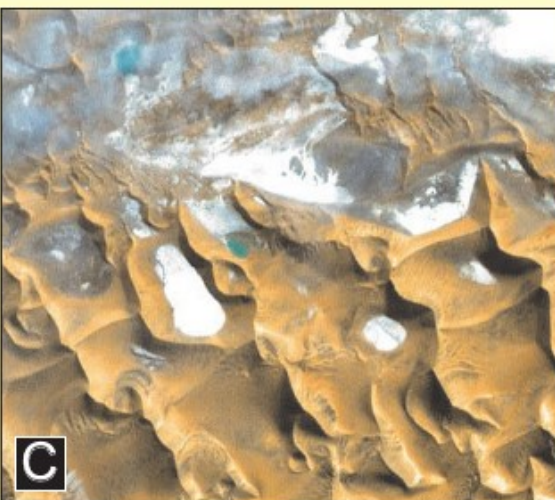
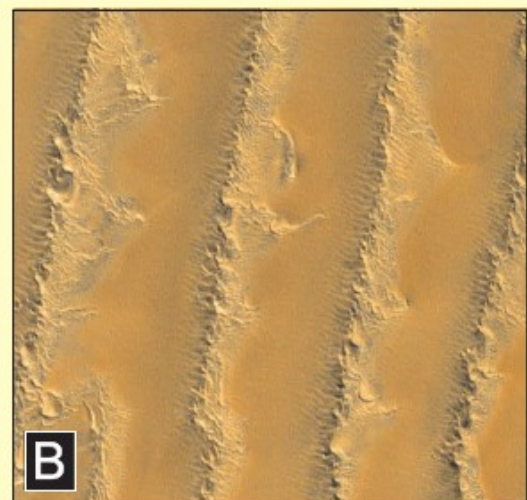
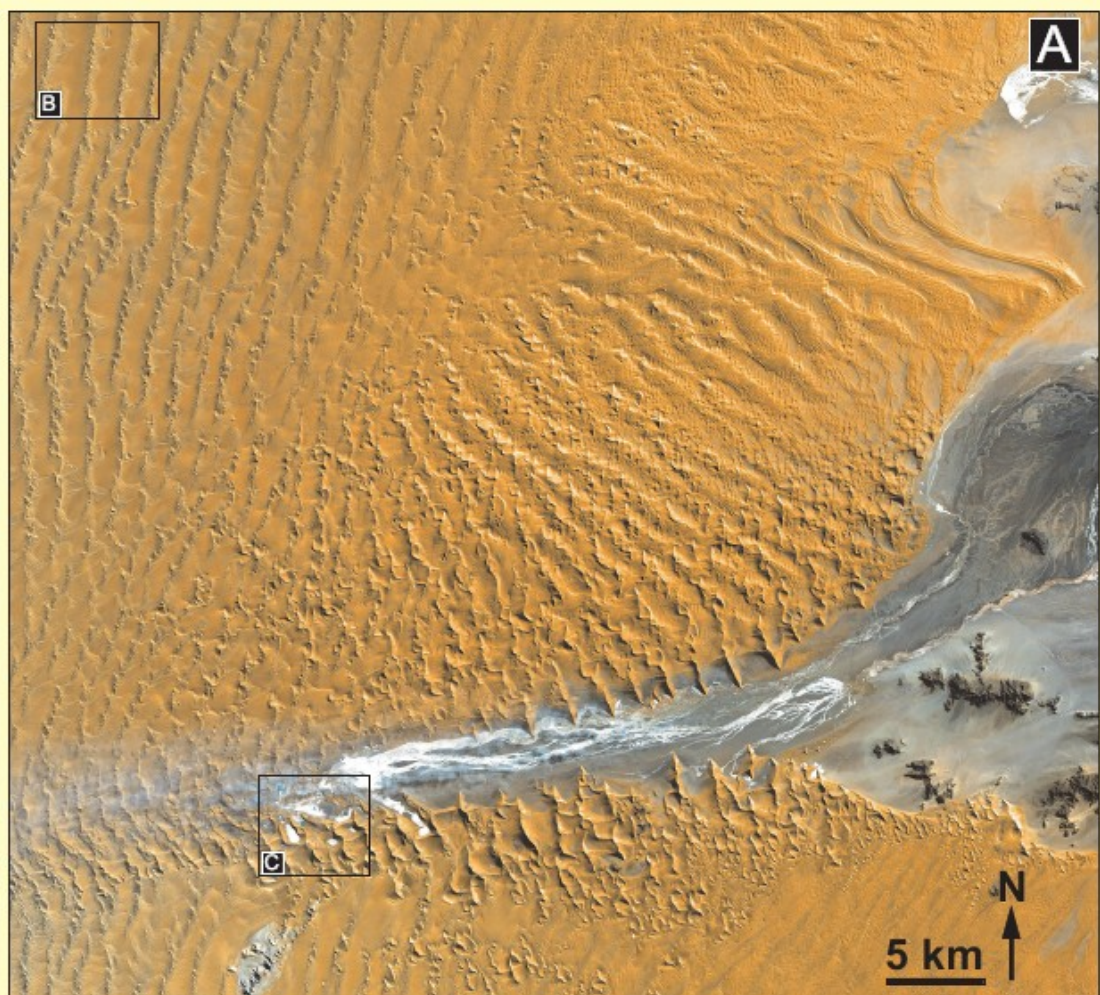


Image of part of the central Namib Desert. A) Separate elements composed of morphologically distinct bedform types are evident. B) Complex linear draa with superimposed transverse dune ribs. Net sand transport is from SSW to NNE. C) Mosaic of pyramid star draa with isolated interdune hollows. White color represents salt and calcrete deposits, green color represents ponded water in wet interdunes. Image courtesy of NASA Earth Observatory collection.

Mountney (2006)

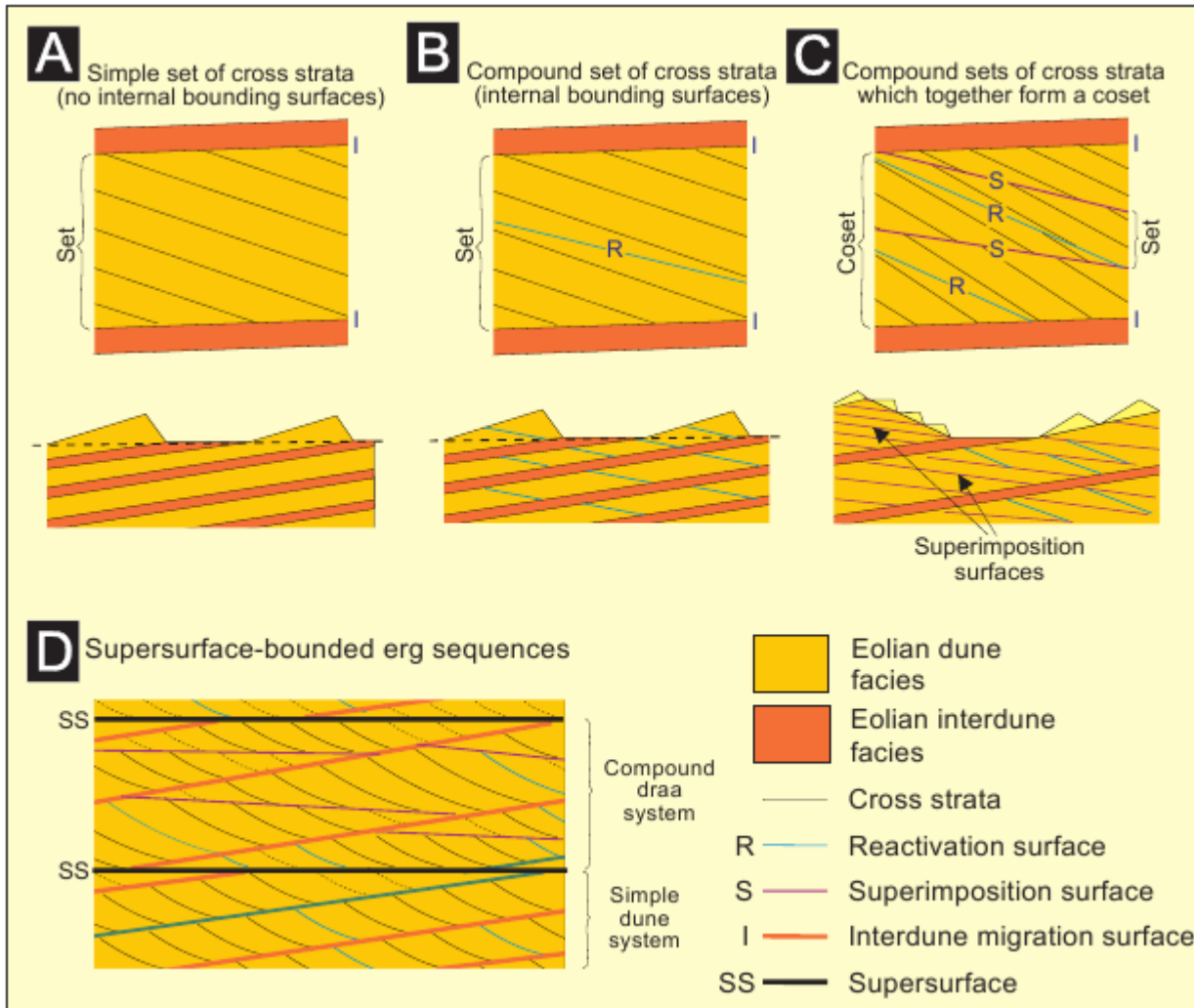


FIG. 30.—Models illustrating the geometry of reactivation surfaces, superposition surfaces, interdune migration surfaces, and supersurfaces in eolian systems. The hierarchical nature of the bounding surfaces, as described by Brookfield (1977), is not always readily identifiable in the rock record. The surfaces do not necessarily break into universally distinct groups by extent or dip angle.

However, higher-order bounding surfaces always truncate lower-order bounding surfaces. Modified after Kocurek (1991).

Mountney (2006)

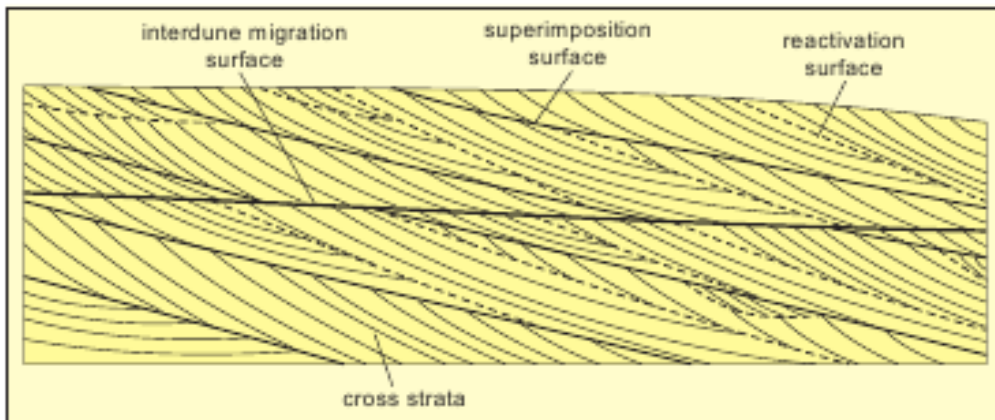


FIG. 31.—Definition diagram for the hierarchical system for describing eolian bounding surfaces in compound-cross-bedded sands and sandstones, as proposed originally by Brookfield (1977). Interdune migration surfaces arise as a consequence of dune migration. Superimposition surfaces represent the migration of superimposed bedforms and/or scour pits over a larger parent bedform. Reactivation surfaces represent partial deflation of a bedform lee slope and arise in response to periodic changes in bedform migration direction, steepness, speed, and/or asymmetry.

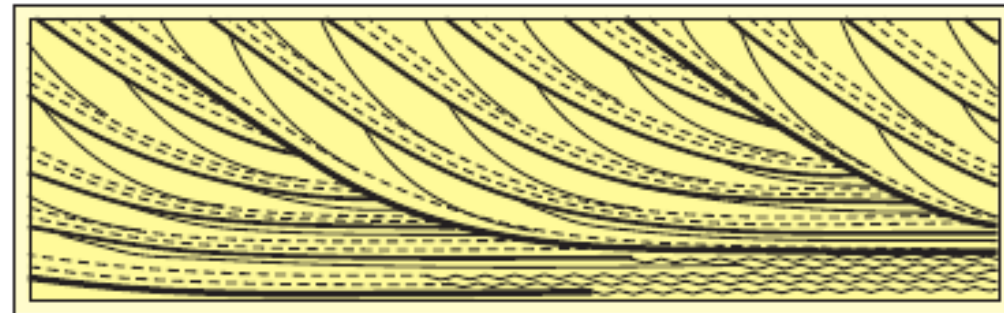


FIG. 32.—Schematic diagram illustrating a co-set of scalloped cross strata with internal cyclicity. Two distinct scales of bounding surface are evident within the co-set. Note how bounding surfaces at the base of the sets pass down dip into corrugated surfaces. This relationship, which can potentially occur at a variety of scales, is indicative of eolian dune migration that occurs synchronously with accumulation in damp, water-table-controlled interdunes. Based on observations from the Jurassic Entrada Sandstone, NE Utah, U.S.A. Modified from Crabaugh and Kocurek (1993).

Mountney (2006)

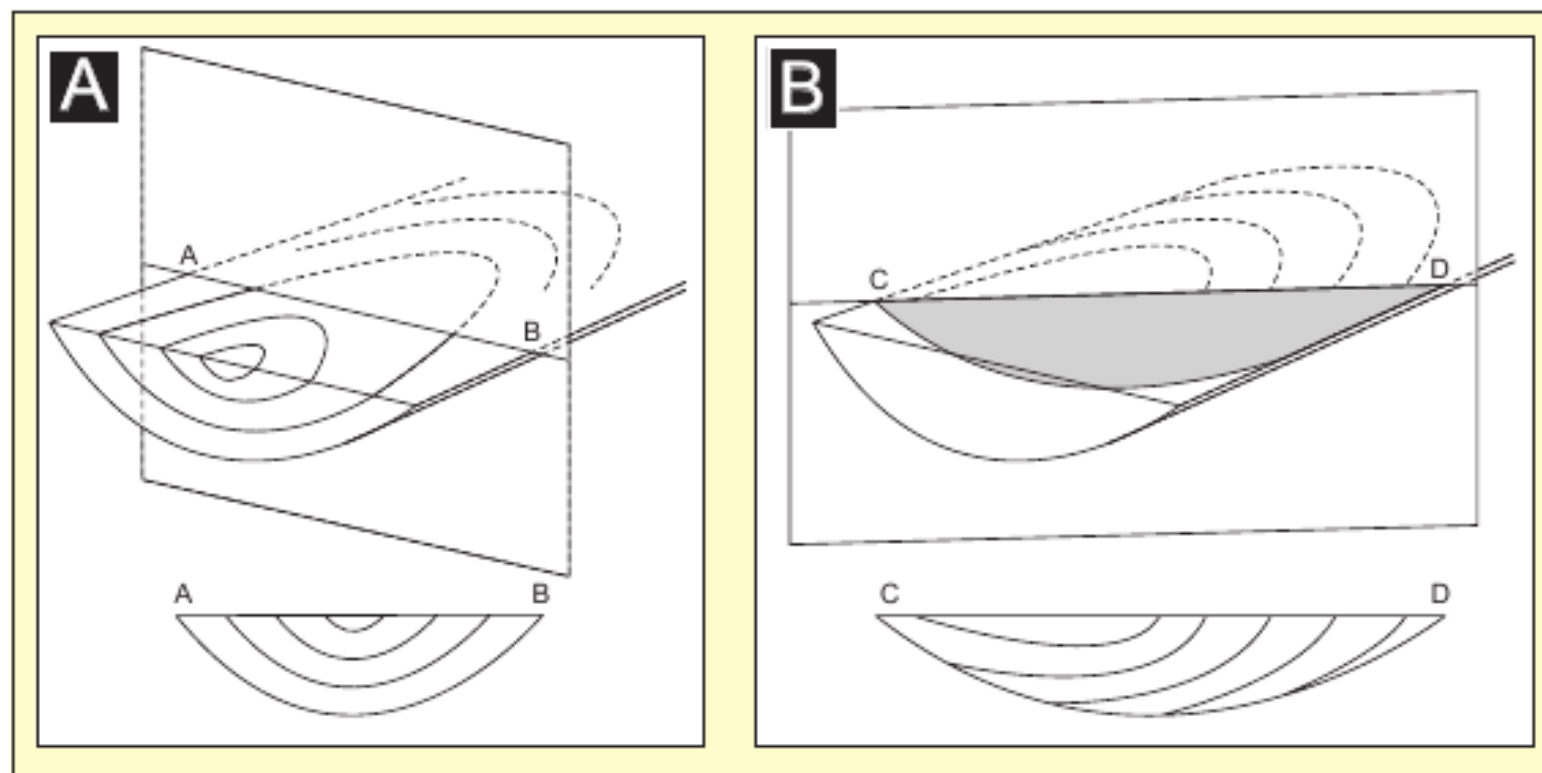


FIG. 34.—Schematic illustration of the geometric complexity of trough-cross strata. **A)** A vertical section oriented transverse to the trough axis reveals symmetrical cross-stratification planes that are apparently concordant with the trough base. **B)** A vertical section oriented oblique to the same trough axis reveals cross-stratification planes that apparently fill the trough asymmetrically and downlap onto its base. This illustrates the problems associated with the measurement of foreset dip azimuths from core or outcrop for the purposes of establishing paleo-transport direction from trough-shaped cross strata. Modified after DeCelles et al. (1983).

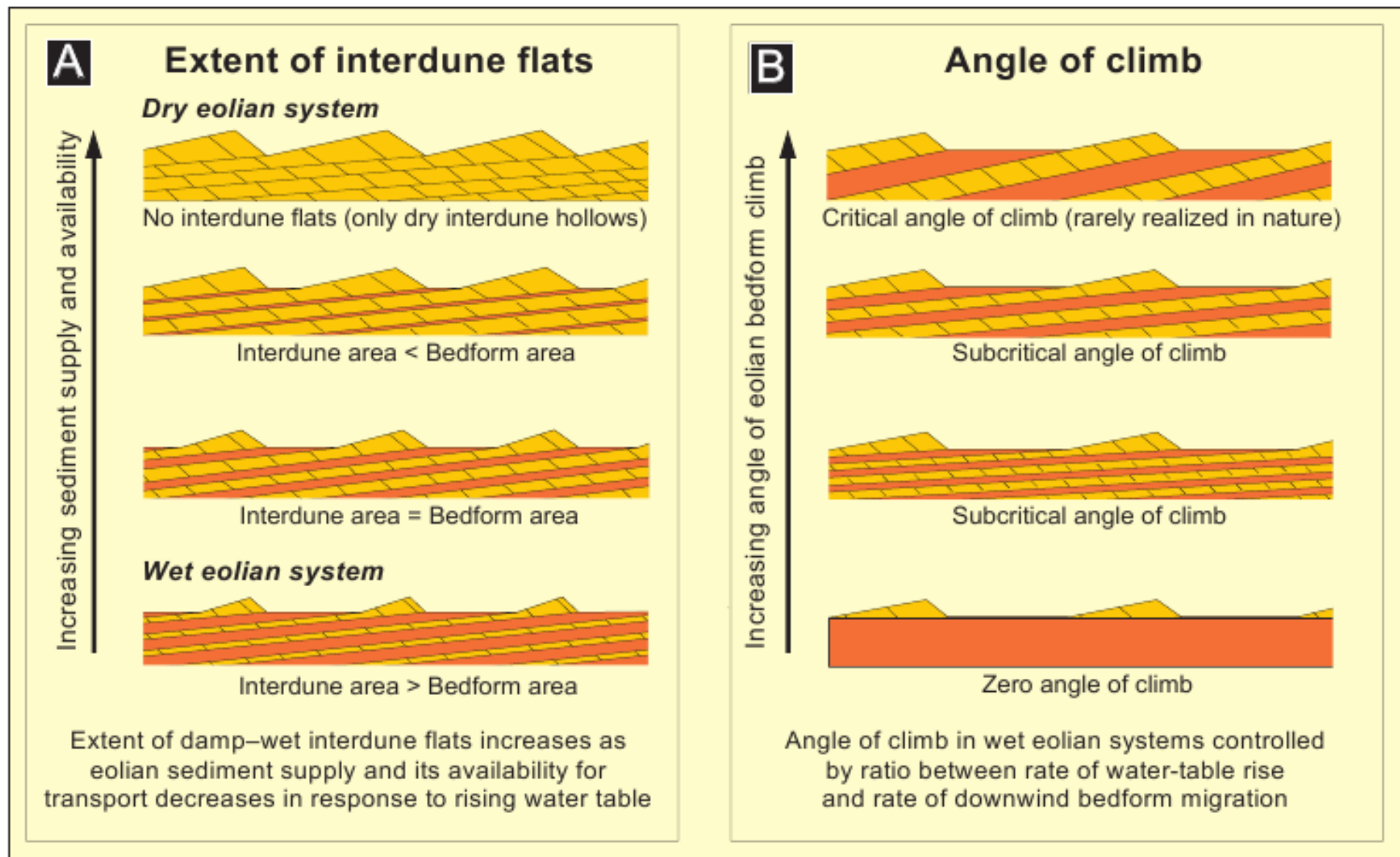


FIG. 61.—Basic controls on interdune geometry in wet eolian systems. Modified in part from Kocurek and Havholm (1993).

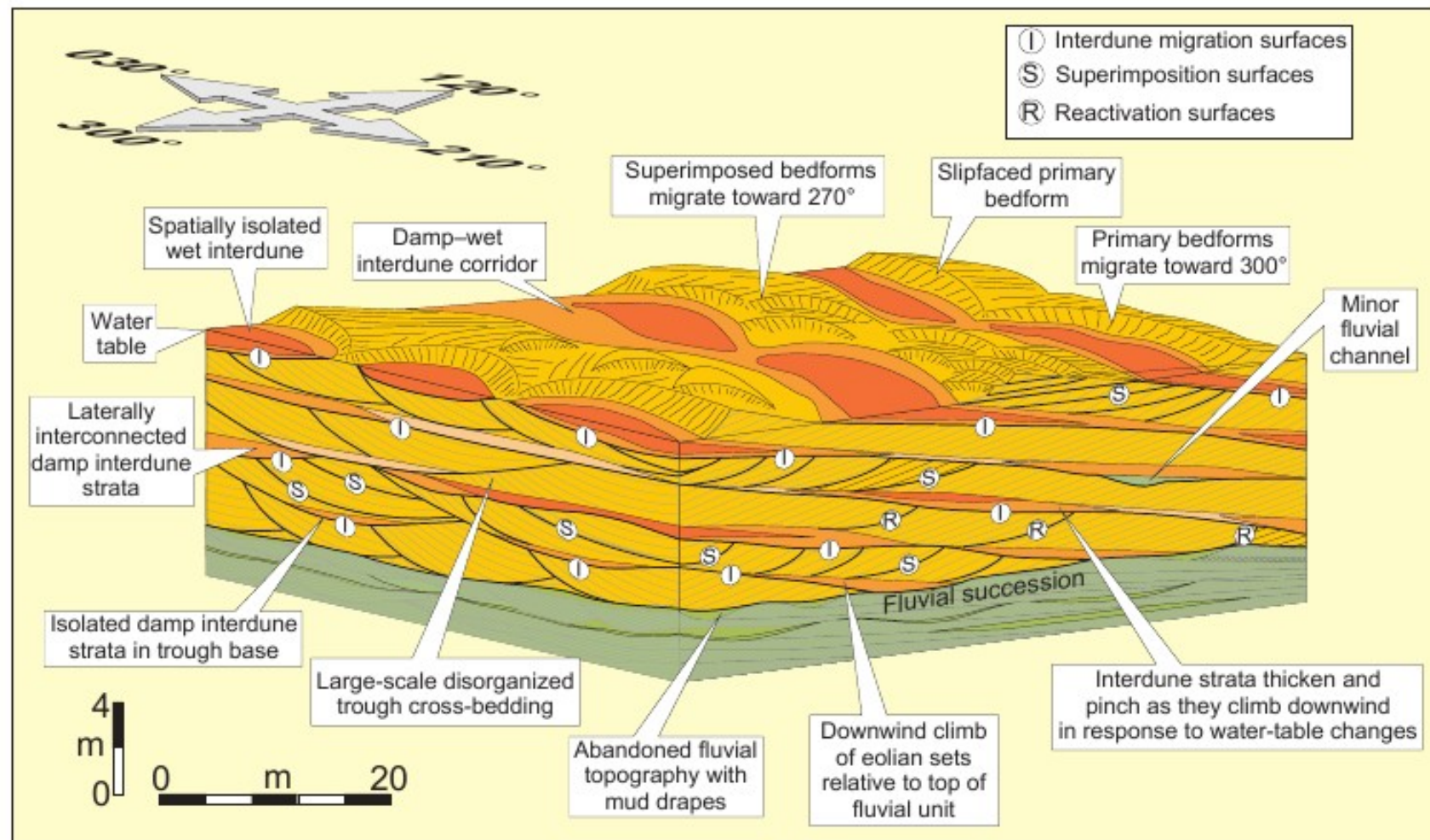


FIG. 55.—Depositional model for the Triassic Helsby Sandstone Formation, Cheshire Basin, UK. Dune elements climb downwind, as do adjacent interdune elements, which exhibit downwind facies variability that reflects subtle changes in the level of the water table relative to the accumulation surface during accumulation. Lateral connectivity of the interdune elements is controlled by dune morphology, and both isolated interdune hollows (ponds) and interconnected, throughgoing corridors are recognized. Modified after Mountney and Thompson (2002).

# Eólico Pré-Cambriano

Mais antigos depósitos eólicos - . 2.1 Ga Deweras Group (Zimbabwe) and Hurwitz Group I (Canada).

Diversos exemplos a partir de 1.8 Ga

Ausência de depósitos arqueanos e escassez pré 1.8 Ga -

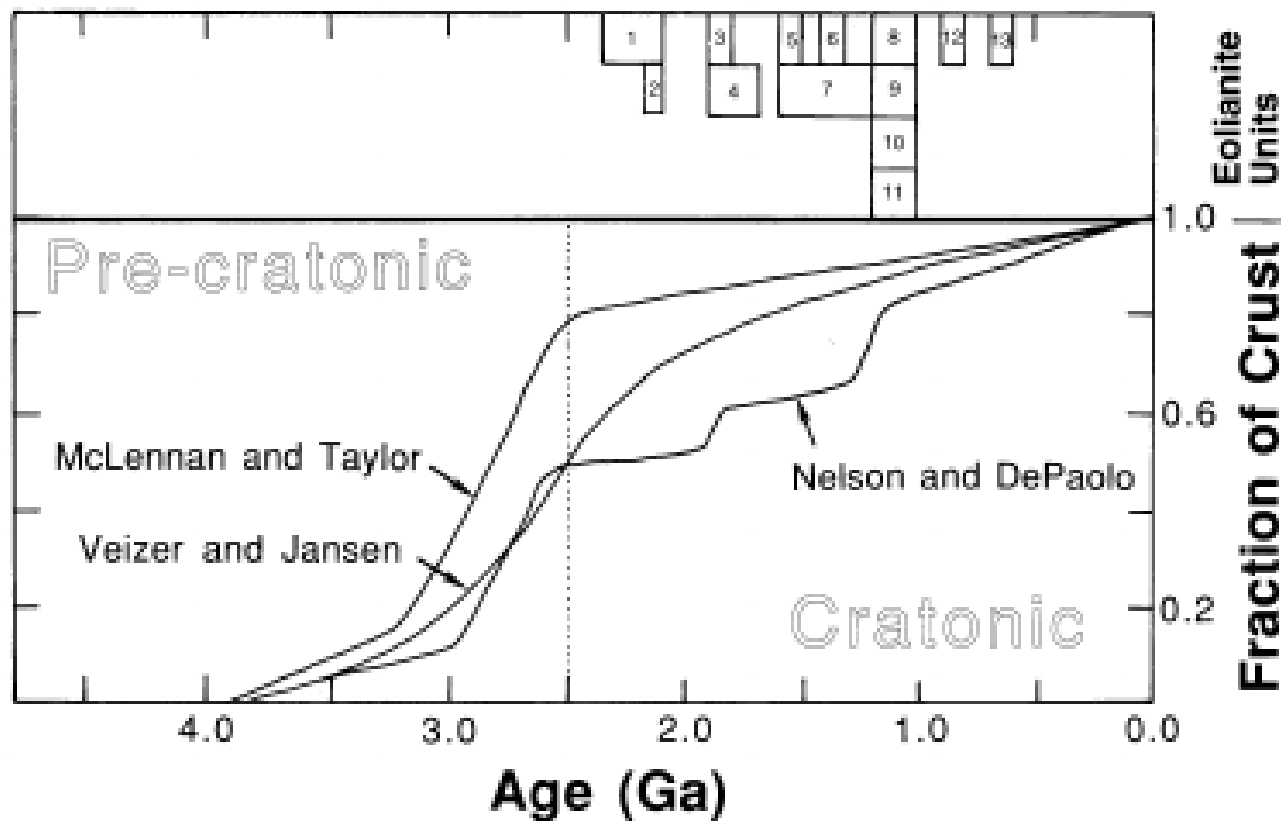
- crescimento crustal

- atmosfera menos densa? Não – depósitos fluviais implicam em chuva desde o

Arqueano

- não reconhecimento

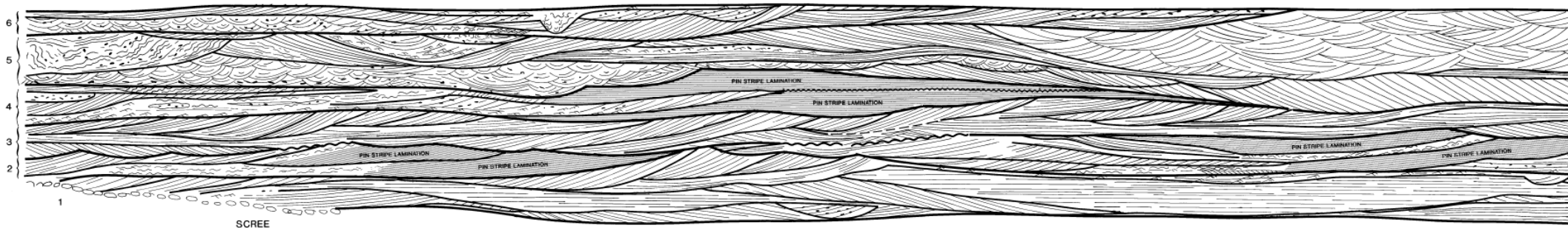
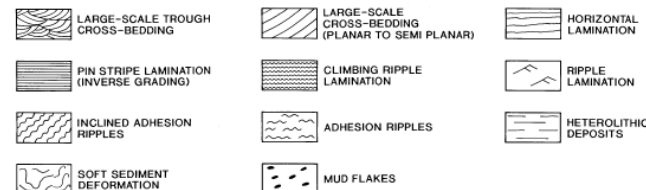
Abundância após 1.8 G.a. - estabelecimento dos ciclos de supercontinentes.



Eriksson &amp; Simpson (1998)

Crustal growth models and temporal distribution of eolian deposits; ages of deposits are rounded to 100 million years. Precratonic (greenstone) sedimentary successions dominate the pre-2.5-Ga record. Cratonic sedimentary successions are mostly younger than 2.5 Ga. Curves are from Veizer and Jansen (1979), McLennan and Taylor (1982) and Nelson and DePaolo (1985). Eolianite units shown and the sources of their ages are: 1 D Hurwitz Group, Canada (Aspler et al., 1992); 2 D Deweras Group, Zimbabwe (Master, 1991); 3 D Makgabeng Formation, South Africa (Tankard et al., 1982); 4 D Mount Isa Inlier, Australia (Page, 1983a,b); 5 D Hornby Bay Group and Thelon Formation, Canada (Ross, 1983a,b; Jackson et al., 1984); 6 D Dala Sandstone, Sweden (Patchett, 1978); 7 D Nebraska subsurface, U.S.A. (Carlson et al., 1992); 8 D Hazel Formation, U.S.A. (Walker, 1992); 9 D Calyie Formation, Australia (Goode and Hall, 1981); 10 D Copper Harbor Formation, U.S.A. (Taylor and Middleton, 1990); 11 D Mancheral Quartzite and Venkaṭpur Sandstone, India (Chakraborty, 1991; Chakraborty and Chaudhuri, 1993); (12) Bakoye 3 Formation, Morocco (Deynoux et al., 1989).

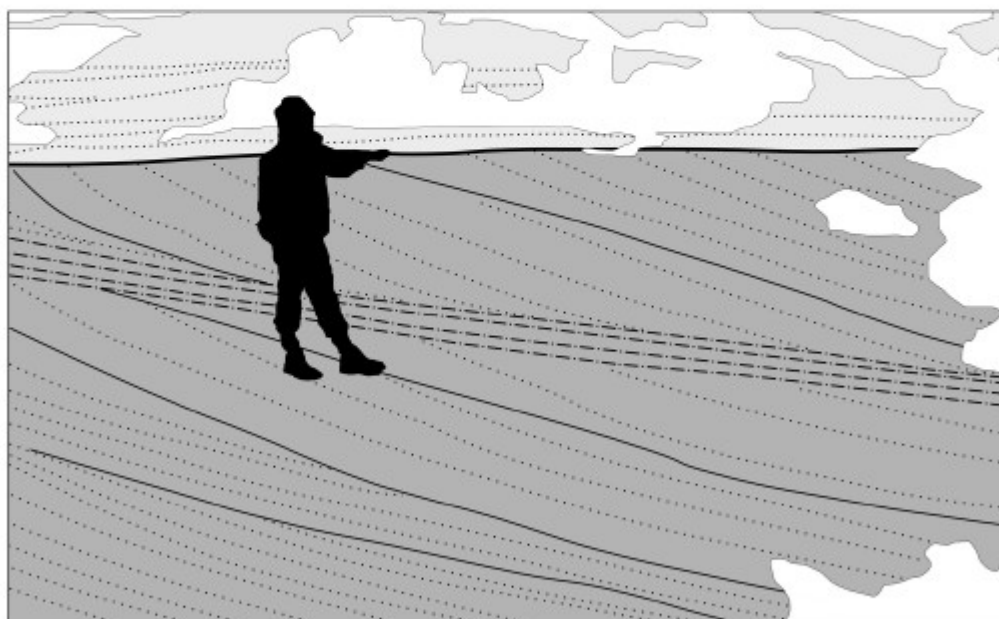
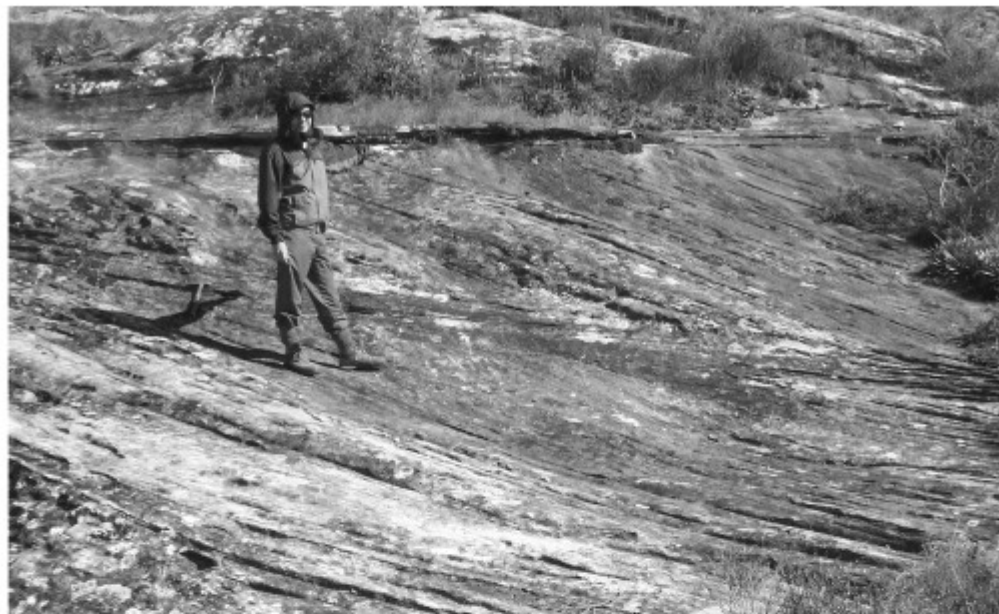
- Preservação de depósitos eólicos pré-vegetação
  - Ocorrência mais abrangente (vegetação ausente)
  - Preservação – controle climático?

**A****B****LEGEND:**

Tirsgaard &amp; Oxnevad (1998)

Fig. 5. (A) Lateral profile of Type I and Type II sand sheets (location is shown in Fig. 2). The profile shows six stacked sand sheets of which 5 and 6 are Type I sand sheets dominated by medium-scale trough cross-bedding. Sand sheets 1–4 are of Type II, showing the typical interbedding of aeolian and fluvial deposits, with aeolian deposits being preserved preferentially on the lee side of fluvial cross-beds. Type II sand sheets are dominated by low-angle and high-angle tabular cross-strata. (B) Multistorey sheet sandstone body consisting of five stacked Type III sand sheets showing the typical architecture of these sand sheets, with relatively planar lower set boundaries and dominance of planar-parallel lamination and climbing ripple lamination with some low-angle cross-strata.





Interdune deposits



Eolian dunes deposits

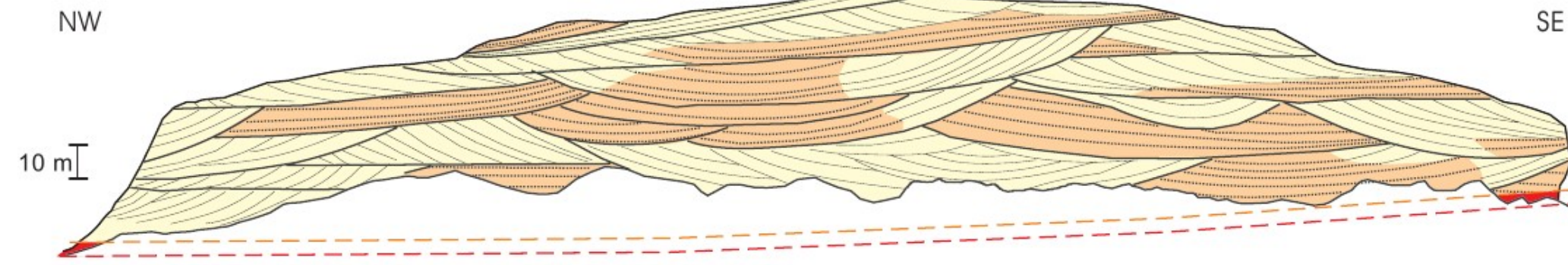
1<sup>st</sup> order surfaces2<sup>nd</sup> order surfaces3<sup>rd</sup> order surfaces

Depositional surfaces

successão eólica superior

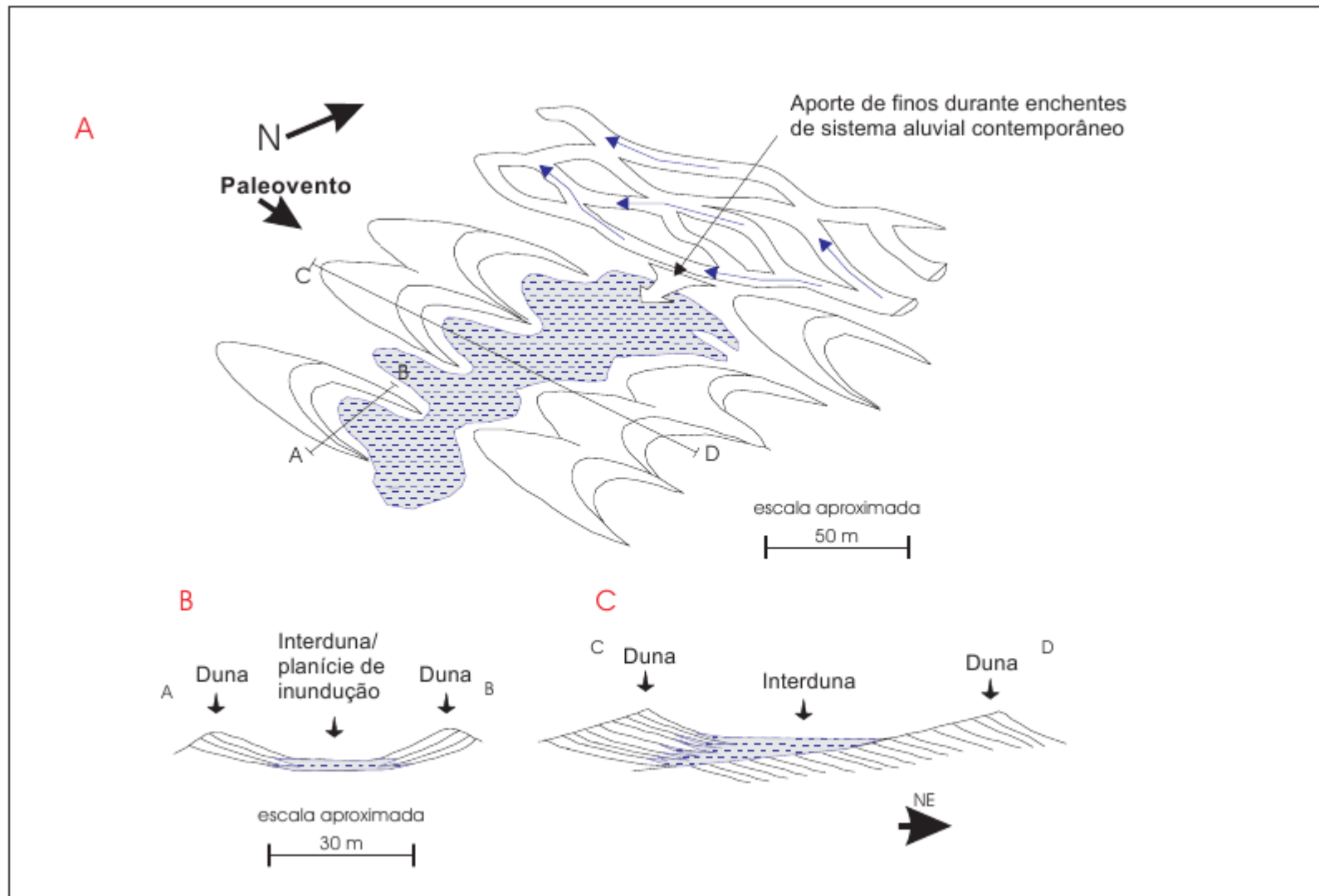


successão eólica inferior



- Superfícies de 1º ordem - cavaleamento de dunas ou interdunas sobre dunas
- ..... Superfícies deposicionais de interdunas úmidas
- Superfícies deposicionais (estratos frontais de dunas) e de 3º ordem (reativações)
- - - Superfícies de reinício da deposição eólica (S4D)
- - - - Supersuperfície, afogamento do campo de dunas (S4C)

- Associação de fácies de dunas eólicas
- Associação de fácies de interdunas-planícies de inundação
- Associação de fácies flúvio-lacustres



- Clemmensen, L. D. & Abrahamsen, K. (1983), 'Aeolian stratification and facies association in desert Arran basin (Permian), Scotland', *Sedimentology* **30**, 311-339. sediments,
- Eriksson, K. A. & Simpson, E. L. (1998), 'Controls on spatial and temporal distribution of Precambrian *Sedimentary Geology* **120**, 275-294. eolianites',
- Kocurek, G. (1996), Desert aeolian systems, *in* H. G. Reading, ed., 'Sedimentary environments, processes, stratigraphy', Oxford. Blackwell Science, , pp. 125-153. facies and
- Kocurek, G. (1988), 'First order and super bounding surfaces in eolian sequences – bounding surfaces *Sedimentary Geology* **56**, 193-206. revisited',
- Kocurek, G. & Dott, R. H. J. (1981), 'Distinctions and uses of stratification types in the interpretation of eolian *Journal of Sedimentary Petrology* **51**(2), 579-595. sands',
- Langford, R. P. (1989), 'Modern and ancient fluvial-eolian interactions: Part1, Modern systems', *Sedimentology* **36**, 1023-1035.
- Langford, R. P. & Chan, M. A. (1989), 'Modern and ancient fluvial-eolian interactions: Part 2, Ancient systems', *Sedimentology* **36**, 1038-1051.
- Marconato, A.; Almeida, R. P.; Santos, M. G. M.; Nóbrega, J. E. S. & Souza, R. B. (2009), 'Alluvial-eolian interaction in a Cambrian rift margin: the Pedra das Torrinhas and Pedra Pintada formations (Guaritas Group, RS)', *Anais da Academia Brasileira de Ciências* **81**(4), 819-836.
- Mountney, N. P. (2006), *Facies Models Revisited*, SEPM, chapter Aeolian facies models, pp. 23-83.
- Paim, P. S. G. & Scherer, C. M. S. (2007), 'High-resolution stratigraphy and depositional model of wind- and water-laid deposits in the ordovician Guaritas rift (Southernmost Brazil)', *Sedimentary Geology* **202**, 776-795.
- Tirsgaard, H. & Oxnevad, I. E. I. (1998), 'Preservation of pre-vegetational fluvio-aeolian deposits in a humid climatic setting: an example from the Middle Proterozoic Eriksfjord Formation, southwest Greenland', *Sedimentary Geology* **120**, 295-317.